



# Nr2e3 functional domain ablation by CRISPR-Cas9D10A identifies a new isoform and generates retinitis pigmentosa and enhanced S-cone syndrome models



Izarbe Aísa-Marín<sup>a,b,c</sup>, M. José López-Iniesta<sup>a,d</sup>, Santiago Milla<sup>e</sup>, Jaume Lillo<sup>f,g</sup>, Gemma Navarro<sup>g,h</sup>, Pedro de la Villa<sup>e,i</sup>, Gemma Marfany<sup>a,b,c,\*</sup>

<sup>a</sup> Department of Genetics, Microbiology and Statistics, Avda. Diagonal 643, Universitat de Barcelona, Barcelona 08028, Spain

<sup>b</sup> CIBERER, ISCIII, Universitat de Barcelona, Barcelona, Spain

<sup>c</sup> Institute of Biomedicine (IBUB, IBUB-IRSJD), Universitat de Barcelona, Barcelona, Spain

<sup>d</sup> MaRCU - Molecular and RNA Cancer Unit, Graduate School of Medicine, Kyoto University, Kyoto, Japan

<sup>e</sup> Department of Systems Biology, University of Alcalá, Madrid 28872, Spain

<sup>f</sup> Department of Biochemistry and Molecular Biomedicine, Molecular Neurobiology Laboratory, Avda. Diagonal 643, Universitat de Barcelona, Barcelona 08028, Spain

<sup>g</sup> CIBERNED, ISCIII, Universitat de Barcelona, Barcelona, Spain

<sup>h</sup> Department of Biochemistry and Physiology, School of Pharmacy, Universitat de Barcelona, Barcelona 08028, Spain

<sup>i</sup> IRYCIS, Madrid, Spain

## ARTICLE INFO

### Keywords:

Nr2e3  
CRISPR  
Cas9D10A nickase  
Retinitis pigmentosa  
Enhanced S-cone syndrome  
Inherited retinal dystrophies  
Mouse models

## ABSTRACT

Mutations in *NR2E3* cause retinitis pigmentosa (RP) and enhanced S-cone syndrome (ESCS) in humans. This gene produces a large isoform encoded in 8 exons and a previously unreported shorter isoform of 7 exons, whose function is unknown. We generated two mouse models by targeting exon 8 of *Nr2e3* using CRISPR/Cas9-D10A nickase. Allele  $\Delta 27$  is an in-frame deletion of 27 bp that ablates the dimerization domain H10, whereas allele  $\Delta E8$  (full deletion of exon 8) produces only the short isoform, which lacks the C-terminal part of the ligand binding domain (LBD) that encodes both H10 and the AF2 domain involved in the *Nr2e3* repressor activity. The  $\Delta 27$  mutant shows developmental alterations and a non-progressive electrophysiological dysfunction that resembles the ESCS phenotype. The  $\Delta E8$  mutant exhibits progressive retinal degeneration, as occurs in human RP patients. Our mutants suggest a role for *Nr2e3* as a cone-patterning regulator and provide valuable models for studying mechanisms of *NR2E3*-associated retinal dystrophies and evaluating potential therapies.

## 1. Introduction

Inherited retinal dystrophies (IRDs) are a group of diseases associated with mutations in more than 330 genes that play critical roles in retinal function (RetNet, the [Retinal Information Network, 1996-2020, https://sph.uth.edu/retnet/](https://sph.uth.edu/retnet/)). Mutations in these genes cause alterations in retinal development or photoreceptor homeostasis, eventually leading to vision loss.

The human retina is formed by rods and three types of cones: S-cones (short wavelength), M-cones (medium wavelength) and L-cones (long wavelength), while the mouse retina is formed by rods, M- and S-cones. Cone photoreceptors mediate colour vision and visual acuity, whereas rod photoreceptors are much more sensitive to light than cones and are excited in dim light conditions (Nathans et al., 1986; Schnapf et al., 1987).

Retinal development requires a careful orchestration of transcription factors (TFs). In mice, retinal progenitor cells (RPCs) divide into post-mitotic photoreceptor precursor cells (PPCs), which express *Otx2* and the downstream target *Crx* to regulate photoreceptor differentiation (Furukawa et al., 1997; Nishida et al., 2003). CRX enhances the expression of photoreceptor-specific genes and is required for terminal rod and cone differentiation (Chen et al., 1997; Freund et al., 1997). CRX interacts with NRL and other TFs to induce the expression of rod-specific genes (Mitton et al., 2000; Mears et al., 2001; Oh et al., 2007; Yoshida et al., 2004). PPCs that do not express *Nrl* follow a default pathway, and differentiate into S-cones unless additional regulatory signals direct them to acquire M-cone identity (Swaroop et al., 2010).

*NR2E3* (or *PNR*, MIM# 604485), an orphan nuclear receptor gene

**Abbreviations:** IRDs, Inherited Retinal Dystrophies; RPCs, Retinal Progenitor Cells; PPCs, post-mitotic Photoreceptor Precursor Cells; *rd7*, retinal degeneration 7; ESCS, Enhanced S-cone Syndrome; RP, Retinitis Pigmentosa

\* Corresponding author at: Department of Genetics, Microbiology and Statistics, Avda. Diagonal 643, Universitat de Barcelona, Barcelona 08028, Spain.

E-mail address: [gmarfany@ub.edu](mailto:gmarfany@ub.edu) (G. Marfany).

<https://doi.org/10.1016/j.nbd.2020.105122>

Received 5 June 2020; Received in revised form 23 September 2020; Accepted 25 September 2020

Available online 30 September 2020

0969-9961/ © 2020 The Author(s). Published by Elsevier Inc. This is an open access article under the CC BY-NC-ND license (<http://creativecommons.org/licenses/by-nc-nd/4.0/>).

expressed in the retina (Kobayashi et al., 1999), is a direct transcriptional target of NRL (Oh et al., 2008). NR2E3 forms a complex with NRL and CRX to enhance the expression of rod genes and suppress the expression of cone genes, allowing rod maturation (Chen et al., 2005; Cheng et al., 2006; Peng et al., 2005). NR2E3 has a dual role in rod and cone differentiation since it can function as both a transcriptional activator and a repressor. Therefore, it is necessary for cone gene inhibition and rod maturation during retinal development, and in addition, it is also relevant for photoreceptor homeostasis and is expressed at high levels in the adult retina (Cheng et al., 2004; Haider et al., 2001).

NR2E3 is a ligand-regulated transcription factor whose physiological ligands are unknown (Kobayashi et al., 1999; Qin et al., 2013). It shares the protein structure displayed by nuclear receptors consisting of a N-terminal DNA-binding domain (DBD) and a C-terminal ligand-binding domain (LBD) formed by a hydrophobic pocket of 12 helices (Tan et al., 2013). The reported active form of NR2E3 is homodimeric, and dimerization is mediated by the helix 10 domain (H10) located in the LBD and close to the protein C-terminus (Tan et al., 2013). Structural modeling based on the LBD crystal structure revealed an auto-repressed conformation in which the activation-function-2 helix (AF2) occupies the canonical cofactor binding site, which is thus required for the NR2E3 transcriptional repressor activity (Kanda and Swaroop, 2009; Tan et al., 2013). TFs are usually modulated by reversible post-translational modifications, for instance, NR2E3 sumoylation is required to repress cone genes, whereas the non-sumoylated NR2E3 mainly acts as a trans-activator of rod genes (Onishi et al., 2009). In humans, this gene produces a large transcript isoform that spans 8 exons (NM\_014249.4) and produces the conventional NR2E3 protein (410 aa, NP\_055064.1). A shorter transcript isoform (NM\_016346.4) retains intron 7 and thus generate a shorter protein of 367aa (NP\_057430.1) that lacks exon 8, which encodes the dimerization H10 and AF2 helices. The physiological function of this shorter isoform is yet to be determined.

NR2E3 mutations cause either retinitis pigmentosa (RP, MIM# 611131) or enhanced S-cone syndrome (ESCS; MIM# 268100), whose most severe affection is also named Goldmann-Favre syndrome (GFS; MIM# 26800), generally in recessive forms (Bernal et al., 2008; Coppieters et al., 2007; Escher et al., 2009; Favre, 1958; Gire et al., 2007; Haider et al., 2000; Schorderet and Escher, 2009). RP is characterized by progressive loss of rod photoreceptors, thus producing decreased peripheral vision and night vision loss, followed later by cones. ESCS instead is characterized by an excess of S-cones in detriment of rods, whose function is also altered, most probably due to mutated NR2E3 failure in repressing cone genes during retinal development (Haider et al., 2000). Phenotype-genotype correlation is well established for the p.G65R mutation, the only dominant pathogenic NR2E3 variant, which is associated with autosomal dominant RP (adRP, RP37) (Coppieters et al., 2007; Gire et al., 2007). However, there is no clear phenotype-genotype correlation for recessive retinal dystrophies associated to NR2E3 mutations, which suggest different disease mechanisms (Schorderet and Escher, 2009).

Animal models are extremely useful tools to study the disease mechanisms at the molecular and morphological level. The *retinal degeneration 7 (rd7)* mouse has been used as a natural model of ESCS. An insertion of a L1 retrotransposon in exon 5 of *Nr2e3* causes aberrant splicing and absence of protein in the *rd7* mouse retina (Akhmedov et al., 2000; Haider et al., 2001; Chen et al., 2006). However, some authors question *rd7* as a complete model of the human disease due to some discordances between mouse and human functional tests (Schorderet and Escher, 2009). Knockout lines of *Nr2e3* have been generated in mice (Webber et al., 2008) and zebrafish (Xie et al., 2019) resembling some of the phenotypic features found in the *rd7* retina. Even so, the molecular mechanisms causing the diverse phenotypes of NR2E3-associated pathologies are still unknown.

As mentioned, the shortest NR2E3 isoform lacks the H10 and AF2

domains encoded in exon 8. On the other hand, a number of NR2E3 mutations that cause retinal dystrophies map at exon 8 (Supplementary Table 1, based on the Human Gene Mutation Database (HGMD, 2017; <https://www.hgmd.cf.ac.uk>). In order to dissect the role of the two isoforms in *Nr2e3* function and elucidate their contribution to the retinal disorders caused by NR2E3 mutations, we have used CRISPR-Cas9 gene editing to delete exon 8 in mouse. Several modified alleles that altered the sequence of the last exon, thereby affecting the C-terminal domains, were produced and we obtained homozygous mice for careful phenotypic analysis. In the present work we present the generation and phenotype characterization of two novel *Nr2e3* mouse models that show similar phenotypic traits to human disorders. These models will be very useful to study how mutations in NR2E3 alter photoreceptor development, differentiation and survival and lead to either ESCS or RP diseases.

## 2. Material and methods

### 2.1. Animals and ethical statement

Animal handling, euthanasia and surgical dissection was performed according to the ARVO statement for the use of animals in ophthalmic and vision research, following the guidelines for animal care of the University of Barcelona and with the approval of the Bioethics Committee (File number FUE-2019-00965313, ID 2MDLDY4WZ).

### 2.2. Generation of gene-edited mice using the CRISPR/Cas9 system

The CRISPR/Cas9 system was used to generate a *Nr2e3* mouse model by deleting the exon 8 of the locus. To minimize potential off-targets, D10A Cas9, one of the nickase mutants of Cas9, was used. Detailed information on mutant mice generation and genotyping is described in the Data in Brief companion article (Aísa-Marín et al., in press).

### 2.3. RNA isolation and reverse transcriptase PCRs (RT-PCR and qRT-PCR)

WT mouse retinas were homogenized using a Polytron PT1200E homogenizer (Kinematica, AG, Lucerne, Switzerland). Total RNA was isolated using the RNeasy Mini Kit (Qiagen, Germantown, MD) and RNeasy Plus Mini Kit (Qiagen, Germantown, MD), following the manufacturer's instructions with minor modifications (treatment with DNase I during 1 h). Reverse transcription reactions were carried out using the qScriptTM cDNA Synthesis Kit (Quanta BioSciences, Inc., Gaithersburg, MD). Specific primers for amplification were designed and optimized (Supplementary Table 2). RT-PCR was performed according to standard thermocycling conditions. Real-time PCR (qPCR) was performed using LightCycler 480 SYBR Green I Master and a LightCycler 480 Multiwell Plate 384 (Roche Diagnostics GmbH, Penzberg, Germany) in a final reaction volume of 10  $\mu$ l. The levels of gene expression were determined using the comparative Ct method. The Student *t*-test was applied when tests for normal distribution and homodasticity rendered positive results.

### 2.4. Protein modeling

Protein modeling was based on the human NR2E3 structure published in the National Eye Institute commons (NEI, 2017, <https://neicommmons.nei.nih.gov>). Swiss-model EXPASY (2017, <https://swissmodel.expasy.org>) was used to align the mouse NR2E3 protein sequence to the human NR2E3 structure taking advantage of the alignment mode. The resulted mouse NR2E3 structure and the location of the different domains were visualized and analyzed using PyMOL software (The PyMOL Molecular Graphics System, Version 1.2r3pre, Schrödinger, LLC).

## 2.5. Cell culture, transient transfection and expression vectors for Bioluminescence Resonance Energy Transfer (BRET) Assays

For BRET assays, sequences encoding fusion proteins consisting of the wild type and the two NR2E3 mutants were fused at the N-terminus of Renilla luciferase (Rluc) and yellow fluorescent protein (YFP) using pRluc-N1 and pEYFP-N1, generously provided by Dr. Francisco Ciruela (Ciruela and Fernández-Dueñas, 2015). *Nr2e3* wild type,  $\Delta E8$  and  $\Delta 27$  coding sequences were amplified by PCR using primers containing the restriction enzyme sites at the 5'-end of Rluc and YFP proteins and lacking the stop codon to obtain the correct in-frame fusion proteins. Primers used can be found in Supplementary Table 2.

Human embryonic kidney (HEK293T) cells were grown in Dulbecco's modified Eagle's medium (DMEM) supplemented with 2 mM L-glutamine, 100  $\mu$ g/ml sodium pyruvate, 100 units/ml penicillin/streptomycin, MEM non-essential amino acid solution (1/100), and 5% (v/v) heat-inactivated fetal bovine serum (FBS) (all supplements were from Invitrogen). Transient transfection was developed with PEI method and BRET assays were performed as previously described (Reyes-Resina et al., 2020). Data were fitted to a nonlinear regression equation, assuming a single-phase saturation curve with GraphPad Prism software. BRET is expressed as milliBRET units (mBU).

## 2.6. Immunostaining of whole mount retinas and cone counting

Mice were sacrificed by cervical dislocation, the eye was enucleated immediately after death and placed in  $1 \times$  PBS. A small hole in the cornea was performed with a needle to allow a 4% PFA solution (in  $1 \times$  PBS) entering into the eye for 10 min. The iris was cut to remove the cornea and the lens. The whole retina was dissected from the retinal pigment epithelium and other ocular structures by applying gentle pressure with the Dumont forceps. Careful cuts at the edges were performed to flatten the tissue and the retina was placed with the photoreceptors upside. The retina was transferred to a slide, fixed using 4% PFA in  $1 \times$  PBS for an hour and washed 3 times in  $1 \times$  PBS for 10 min each at room temperature. A solution of 0.1% Triton-X-100 and 5% sheep serum in PBS was used to block the non-specific sites and permeabilize the tissue for 1 h. Alexa Fluor 647-conjugated PNA was incubated for 2 h at room temperature (antibodies and dilutions are specified in Supplementary Table 3). Samples were mounted using Fluoprep (BioMerieux, Marcy-l'Étoile, France) and a coverslide, and stored at 4 °C. Images were obtained by confocal microscopy (SP2, Leica Microsystems; and Carl Zeiss LSM880, Jenna, Germany) and analyzed by ImageJ. The number of cones per area was quantified in regions of interest (ROI) placed randomly across the whole retina. Three ROIs of the same area (6.543,895 square microns) were placed in each picture of the retina, and we took 10–15 pictures per retina. For 2.5 D views, the ZEN 2.1 software (Zeiss microscopy) has been used to convert intensity values of two dimensional images into a height map in the z-axis. For statistical analysis R studio software was used. Two-Way ANOVA was applied when tests for equal standard deviation (SD) and normal distribution rendered positive results.

## 2.7. Immunostaining of mouse retinal sections

The procedure for dissecting the mouse neuroretina and eyecup was previously described (Toulis et al., 2016). Cryosections of mouse retinas (10–12  $\mu$ m slides) were obtained using a Leica CM3050-S cryostat. Slides were thawed at room temperature for 10 min, washed in X1 PBS for 5 min and incubated in PBST (0.5% Triton-X-100 in PBS) for 15 min. Then, they were washed 3 times in  $1 \times$  PBST for 5 min at room temperature and incubated in blocking buffer (5% sheep serum in  $1 \times$  PBS) for 2 h. All primary antibodies were incubated at 4 °C overnight. After 3 washes in  $1 \times$  PBST for 5 min each at room temperature, PNA, the pertinent secondary antibody and DAPI (1:300 blocking buffer, Roche) were added and incubated for 2 h at room temperature (antibodies and

dilutions are specified in Supplementary Table 3). Slides were washed 3 times in  $1 \times$  PBST for 10 min each at room temperature and mounted using Fluoprep and a coverslide. Samples were kept at 4 °C until confocal microscopy (SP2, Leica Microsystems; and Carl Zeiss LSM880).

## 2.8. Transmission electron microscopy (TEM)

Three animals per group (12 months-old) were used. Eyes from wild type,  $\Delta E8$  and  $\Delta 27$  were enucleated, the cornea was perforated using a needle to create a small hole and eyes were immersed in fixative solution (2.5% glutaraldehyde, 2% PFA in 0.1 M phosphate buffer) incubation at 4 °C overnight. After several rinses (0.1 M phosphate buffer) using a shaker, eyes were post-fixed in 1% osmium tetroxide and 0,8%  $K_4Fe(CN)_6$  in the dark for 2 h at 4 °C temperature, rinsed in double distilled water to remove the osmium. Eyes were dehydrated in ascending concentrations of acetone, and embedded in Epon (EMS). Blocs were obtained after polymerization at 60 °C for 48 h. Semithin sections of 1  $\mu$ m in thickness were obtained using a UC6 ultramicrotome (Leica Microsystems, Vienna, Austria), dyed with 0.5% methylene blue and observed in an optic microscope Leica DM200 (Leica Microsystems, Vienna, Austria). Ultrathin sections of 60 nm thick were obtained using a UC6 ultramicrotome (Leica Microsystems, Austria), and stained with 2% uranylless and lead citrate. Sections were observed in a Jeol EM J1010 (Jeol, Japan), and images were acquired at 80 kV with a  $1 k \times 1 k$  CCD Megaview camera.

## 2.9. Morphometric analysis

Semi-thin sections (1  $\mu$ m) for TEM (see previous subsection) of eyes from wild type,  $\Delta E8$  and  $\Delta 27$  mutant mice (three animals per group, 12 months-old) were stained with 0.5% methylene blue. Sections of the central retina (containing the optic nerve) were examined and photographed under the ZOE™ Fluorescent Cell Imager (Bio-Rad, Hercules, CA, USA). The ImageJ software was used for measuring the thickness of the retinal layers at 200  $\mu$ m intervals. Mann-Whitney tests were performed for statistical analysis.

## 2.10. Electroretinography recordings

Young (3–4 months old) and old (7–12 months old) mice were used for each of the three genotypes (wild type, and  $\Delta E8$  and  $\Delta 27$  homozygotes). Electroretinography recordings were performed in 5–8 animals per group. Dark-adapted animals were anaesthetized with an intraperitoneal injection of saline solution (NaCl 0.9%), containing ketamine (70 mg/kg) and xylazine (7 mg/kg). Before recording, pupils were dilated with one to two drops of 1% tropicamide (Alcon, Spain). To preserve the corneal surface from desiccation, a drop of 2% methylcellulose was applied (Methocel, Switzerland). Three recording electrodes (ground, reference, and corneal) were used (Burian-Allen, Hansen Ophthalmic Development Lab, Coralville, IA). In all experiments, animal handling was performed under indirect dim red light (> 620 nm) and mice were kept at 37 °C on a heating pad during the entire procedure. For low-intensity ( $-2 \log$  Cds/m<sup>2</sup>), a single light-emitting diode was placed close to the eye. The recorded electrophysiological response was amplified and filtered (CP511 AC amplifier; Grass Instruments, Quincy, MA), and digitalized (ADInstruments Ltd., Oxfordshire, UK). Rod (b-scot), mixed (a-wave and b-wave), and oscillatory potential (OP) responses were recorded sequentially under dark background conditions, and cone (b-phot) responses were recorded following light-adaptation with background white light (50 Cd/m<sup>2</sup>). To test the effect of reducing metabolic stress by illumination, animals were light-adapted for 5 min (50 Cd/m<sup>2</sup>), and then the scotopic mixed response was recorded at different times in scotopic conditions. Rod response amplitude was measured from baseline to the peak from the scotopic recordings; the a-wave amplitude was measured from baseline to the first trough from the mixed response or to the response

amplitudes at 3 and 8 msec, and the b-wave and cone response amplitudes from the first trough to the peak from the mixed (b-wave) and photopic (b-phot) responses. OP was determined as the maximum amplitude between the trough and the peak of the waves. For statistical analysis, data are presented as mean  $\pm$  standard deviation (SD). The significance of the differences between genotypes was determined with T-Student tests.

### 3. Results

#### 3.1. *Nr2e3* mutants generated by CRISPR-Cas9 gene editing on exon 8 confirm the production of an alternative isoform that encodes a shorter NR2E3 protein isoform

To dissect the physiological function of the NR2E3 domains encoded in exon 8 and the function of the shorter protein isoform, we designed the deletion of exon 8 of *Nr2e3* using the CRISPR-Cas9 system. In order to minimize potential off-target effects, we opted for the Cas9 D10A nickase variant, which requires the use of two guide RNAs per site (guide design and position, described in the Data in Brief companion article, Aísa-Marín et al., in press). We thus microinjected the mRNA of the Cas9 nickase plus four different guide RNAs in mouse zygotes to generate double strand breaks (DSBs) at each side of *Nr2e3* exon 8, encoding the C-terminal part of the LBD (Fig. 1A). This strategy generated several modified alleles that altered the sequence of exon 8 (around one third of the resulting chimeric embryos carried at least one modified allele). Binding and recognition of the PAM site by each of the 4 RNA guides was most probably not simultaneous, and according to our results, the upstream sequences were more prone to be cut and repaired, so that most of these gene-edited alleles were only modified at the junction of intron 7 with exon 8 (Data in Brief companion article, Aísa-Marín et al., in press). We generated heterozygous and homozygous strains of two selected alleles, carrying a medium and a short size deletion. The  $\Delta E8$  showed a complete deletion of exon 8 and the 3'-UTR (799 nucleotides, Fig. 1A and B). The  $\Delta E8$  allele cannot encode neither the H10 (necessary for dimerization) nor AF2 (necessary for transcriptional repression) domains. We also selected the  $\Delta 27$  allele, which displays an in-frame deletion of 27 nucleotides (Fig. 1A and C) that ablates the H10 domain within an otherwise unmodified exon 8 and 3'UTR. Semi-quantitative RT-PCR revealed two transcript isoforms in the adult wild-type retina (Fig. 1D). Interestingly, immunodetection by western blot of wild type mice revealed two bands for NR2E3 in the wild-type retina. The band of 48 kDa corresponds to the reported full-length isoform spanning the 8 exons of *Nr2e3*. The band of 38 kDa represents a shorter isoform previously unreported in mice (only described as a transcript in humans), which retains intron 7 and produces a shorter protein isoform due to a premature STOP codon introduced early on intron 7 sequence. The production of the short NR2E3 isoform seems restricted to the mature stage, as immunodetection in E18 embryos (when *Nr2e3* expression begins to increase (Cheng et al., 2004)) only detects the long isoform (Fig. 1E). Besides, in E18 retinas, a relatively high percentage of NR2E3 is sumoylated compared to the more mature tissue, pointing to repression of cone genes (Onishi et al., 2009), in accordance to the initiation of rod differentiation (around P0) (Fig. 1E). Expression analysis of NR2E3 protein isoforms in the mutants shows that the  $\Delta E8$  homozygote only expresses the short isoform, whereas the  $\Delta 27$  homozygote expresses both isoforms, although the longer isoform is 9 amino acids shorter (Fig. 1F). Interestingly, both the long and short protein isoform seem to be more expressed in the  $\Delta 27$  homozygote than in wild type retinas.

To test whether the expression of both *Nr2e3* isoforms was regulated during the retinal development, we quantified the long and short isoforms in P10 (when *Nr2e3* expression peaks, according to National Eye Institute commons (NEI, 2017, <https://neicommmons.nei.nih.gov>) and adult murine retinas (P90) by qRT-PCR (Fig. 1G). The relative proportion of the long and short isoforms at both timepoints in wild-type

and  $\Delta 27$  mice is represented in Fig. 1H. The  $\Delta E8$  mutant was not tested for the long isoform since it lacks exon 8 and primers cannot bind. As previously reported, in the wild-type, *Nr2e3* long isoform expression is significantly higher at P10 than in adult retinas, whereas the short isoform slightly increases its expression in the adult (Fig. 1G and H). Surprisingly, in the  $\Delta 27$  mice the expression of the long isoform is nearly undetectable at P10, but it extremely increases in the adult retinas, reaching even higher levels than the wildtype P10 retinas. In contrast, at P10, the short isoform is significantly more expressed in the  $\Delta 27$  mutant than in the wildtype, and it decreases in the adult retina reaching similar levels than those observed in the control (Fig. 1G and H). Finally, in the  $\Delta E8$  retinas, we can observe an increase in the expression of the short isoform in the adult compared to the P10 stages.

Since intron 7 retention for the generation of the short isoform appears to be developmentally regulated and the  $\Delta 27$  mutant shows opposite levels of isoform production compared to wild-type retinas, we performed *in silico* predictions to find potential exonic splicing enhancers (ESEs) using ESE Finder (Cartegni et al., 2003; Smith et al., 2006). A putative ESE is located within the 27 nucleotides deleted in the  $\Delta 27$  mutant (Supplementary Fig. 1). This predicted ESE could recruit splicing factors in the wild-type transcript and favor the splicing event joining exons 7 and 8. The ablation of the predicted ESE in the  $\Delta 27$  homozygote might favor retention of intron 7 and result in higher levels of the short isoform at P10 (Supplementary Fig. 1).

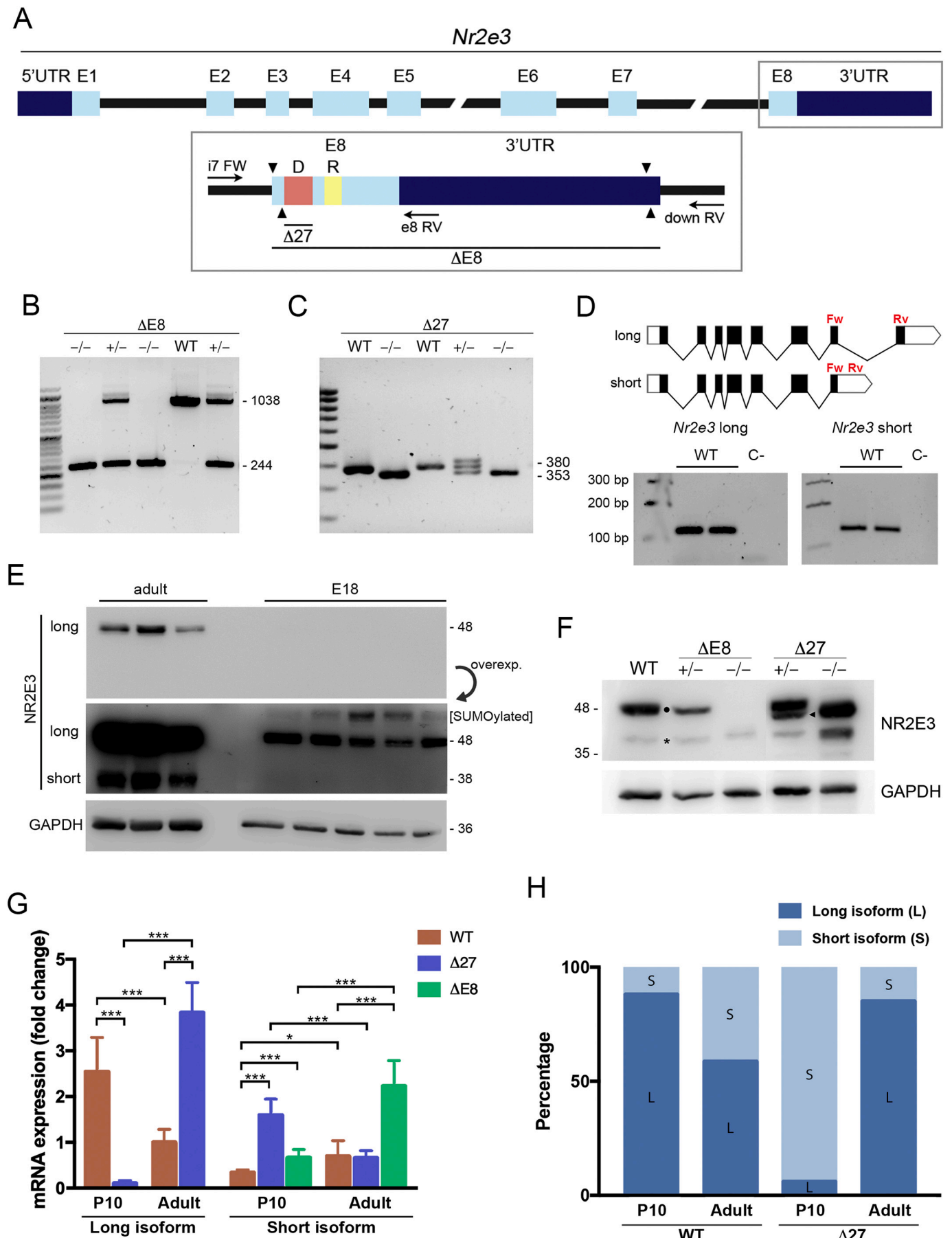
Overall, we hypothesize that the short isoform has a physiological role, since its expression seems to be differentially regulated and intron 7 retention has been identified in transcriptomic analysis at least in humans and mice. The in-frame stop codon at the very beginning of intron 7 is also evolutionary conserved in ten of the eleven vertebrate species considered, pointing to some functionality (Supplementary Fig. 2). This short isoform displays the N-terminal transactivator domain, can bind their target motifs and potentially interact with CRX through the DBD (Peng et al., 2005; von Alpen et al., 2015), but would lack the C-terminal domains H10 and AF2 (respectively involved in the dimerization and repression function of NR2E3), which are highly conserved in all the species analyzed (Supplementary Fig. 2).

#### 3.2. NR2E3 proteins generated after partial in-frame or total deletion of exon 8 show impaired dimerization

Protein modeling visualizes the location of the functional domains ablated in our mutants onto the NR2E3 protein structure (Fig. 2A). The DBD, containing the two zinc fingers and the nuclear localization signal (NLS), is encoded at the N-terminal part of the protein and is thus preserved in our selected alleles. Both deletions affect the LBD, which at the C-terminus displays the H10 and AF2 domains (Fig. 2A).

The known functional form of full-length NR2E3 is a homodimer (Kobayashi et al., 1999), which has been observed in non-denaturing protein gel migration conditions (Roduit et al., 2009), structurally and functionally confirmed by BRET assays (Roduit et al., 2009; von Alpen et al., 2015), DNA binding assays (Escher et al., 2009; Kanda and Swaroop, 2009), as well as the crystal structure of the LBD moiety (Tan et al., 2013).

Disruption of NR2E3 homodimerization has been shown to impair NR2E3 repressor function (Kanda and Swaroop, 2009; Tan et al., 2013). The interaction occurs through the dimerization domain (H10 region) located in the LBD. The  $\Delta E8$  and  $\Delta 27$  alleles lack, completely or partially, the H10 region. Therefore, we assayed the dimerization ability of our mutants by using BRET assay (Fig. 2B), a technique that indicates a physically close molecular interaction. We fused the corresponding coding sequences of each allele and the wild-type sequence (WT) to YFP and Rluc. When expressing a constant amount of NR2E3 WT-Rluc and increasing amounts of NR2E3 WT-YFP, a saturable BRET curve was detected, indicating protein interaction. In contrast, homodimerization of the  $\Delta E8$  and  $\Delta 27$  mutant proteins was greatly impaired, since BRET values were more than one order of magnitude less, thus confirming



(caption on next page)

**Fig. 1.** Generation and molecular characterization of *Nr2e3* mutant alleles by gene editing with CRISPR/Cas9 D10A nickase. A) Schematic representation of the *Nr2e3* wild type gene indicating coding exons (light blue) and 5' and 3'UTRs (dark blue). Below, a magnification of exon 8 shows the encoded dimerization (D) and repressor (R) domains. The  $\Delta E8$  mutant allele presents a full deletion of exon 8 and would result in a shorter protein without the domains encoded in exon 8. The  $\Delta 27$  in-frame mutant lacks 9 amino acids that span the dimerization domain. Black arrows indicate the location of primers used for mice genotyping. Arrowheads indicate the position of the targeting sequences for the four CRISPR guide RNAs (one per each site recognized by Cas9D10A nickases). B) Representative electrophoresis gel with PCR products for  $\Delta E8$  allele genotyping. The 1038 bp band corresponds to the wild type allele whereas the 244 bp band corresponds to the  $\Delta E8$  allele. C) PCR products for  $\Delta 27$  allele genotyping. The 380 bp band corresponds to the wild type allele whereas the 353 bp band corresponds to the  $\Delta 27$  allele. The heterozygous  $\Delta 27^{+/-}$  PCR sample shows three bands corresponding to the two homoduplexes (wildtype-wildtype, mutant-mutant) and the heteroduplex (wildtype-mutant), which has a lower mobility due to secondary structures. D) Reverse-transcription PCR (RT-PCR) of adult retina mRNAs confirming the presence of transcripts for the long and short isoforms. The position of the Forward (Fw) and Reverse (Rv) primers to detect each isoform is indicated. E) Immunodetection by Western blot of several adult and E18 wild-type retinal protein lysates detects the short NR2E3 isoform in the adult retina, but not in the late embryonic stage E18 (when the mouse retina has still only cones). Note the presence of sumoylated NR2E3 protein forms detected in the E18 samples, further supporting the presence of cone gene-repressor forms that enable the rod differentiation pathway (starting around P0). F) Immunodetection of endogenous NR2E3 isoforms in wild type and mutant mouse strains. The 48 kDa band (●) detects the NR2E3 long isoform while the 40 kDa band (\*) detects the NR2E3 short isoform.  $\Delta 27$  mutant shows a slightly shorter size band of 46 kDa reflecting the in-frame deletion of 9 aa (◄). GAPDH was used as loading control. G) Quantification of *Nr2e3* long and short transcript isoforms in the wildtype and mutant retinas by qRT-PCR, considering the expression of the long isoform in the adult wild-type as an arbitrary unit. Two control genes, *Gapdh* and *Actin- $\beta$* , were used for normalization in all samples. For statistical analysis, Student *t*-tests were performed (\*  $p < 0.05$ , \*\*\*  $p < 0.001$ ,  $n = 5-8$  replicates) after testing for normal distribution of the values and homodasticity. Expression of both isoforms is significantly different in the mutants compared to the wildtype at different developmental stages. H) Percentage of the long and short isoform in the wildtype and  $\Delta 27$  mutant in P10 and adults (when the expression of *Nr2e3* peaks) showing that in wild-type mice the long isoform is predominant and decreases with time. In contrast, the  $\Delta 27$  mutant shows opposite expression levels of the two isoforms compared to wild-type. (For interpretation of the references to colour in this figure legend, the reader is referred to the web version of this article.)

that the H10 domain is required for homodimerization of this orphan nuclear factor (Fig. 2A and B).

### 3.3. Homozygous strains of different gene-edited alleles of *Nr2e3* show severe but opposite alterations in the number of cones, and decreased number of photoreceptors

IRDs are frequently characterized by alterations in the number of photoreceptors, and most IRDs show progressive photoreceptor attrition due to a degenerative process, as it occurs in RP. In this respect, ESCS is somewhat exceptional, since it shows a gain—even if dysfunctional—in one specific type of photoreceptors, the S-cones, which are the default differentiation fate from photoreceptor precursors. Consequently, ESCS is characterized by an increase in the number of cones, even though the total number of photoreceptors is decreased, due to the reduced number of rods (Haider et al., 2000; Milam et al., 2002; Schorderet and Escher, 2009; Wright et al., 2004).

Therefore, we aimed to characterize the phenotype of our mutant strains, with a special focus on cone number. We stained retinal whole mounts (> 12 months-old mice,  $n \geq 3$ ) using PNA, a lectin that specifically labels cone membranes and allows the individual visualization of cones (Fig. 3A). Indeed, the total cone number was statistically significantly altered when comparing the retinas of the two mutants with wild type mice (Fig. 3B). The number of cones in the  $\Delta E8$  homozygous mutant retinas was 20% lower than in controls, whereas in the  $\Delta 27$  was 30% higher than in wild type retinas (Fig. 3B). The  $\Delta 27$  heterozygous retinas showed a slight increase (although not significant) in the number of cones, resembling an intermediate phenotype between  $\Delta 27$  homozygous and wildtype retinas (data not shown). Notably,  $\Delta 27$  retinas showed some groups of two and three cones joined by the membrane, as visualized in 2.5D images (pseudo 3D) (Supplementary Fig. 3).

The fact that the two alleles cause an opposite effect in the number of cones suggest that the two homozygous mutant strains could mimic the phenotype of the two different retinal human diseases caused by

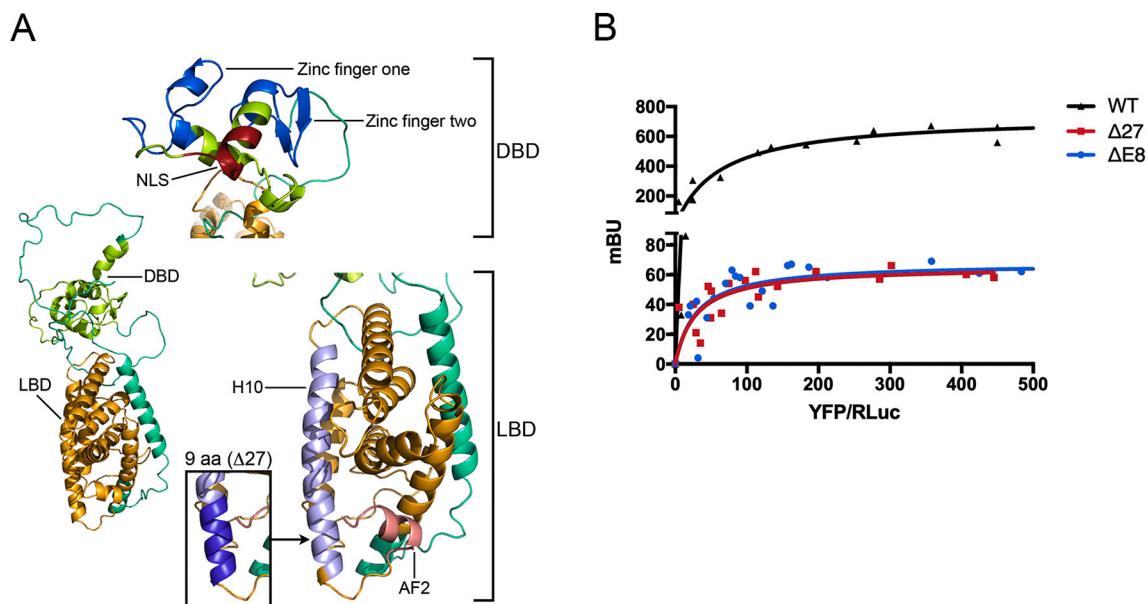


**Fig. 2.** Dimerization of the NR2E3  $\Delta 27$  and  $\Delta E8$  mutant proteins is strongly impaired. A) NR2E3 protein structure showing the DNA binding domain (DBD), which contains the zinc fingers one and two and the nuclear localization signal (NLS), and the ligand binding domain (LBD), which at the C-terminus contains the H10 and AF2 domains, necessary for dimerization and repression activity, respectively. The box highlights the 9 amino acids helix deleted in the  $\Delta 27$  mutant, located at the end of the H10 domain. B) BRET assay results for testing homodimerization of NR2E3 wild type and mutant proteins. Both  $\Delta 27$  and  $\Delta E8$  mutant proteins show nearly full abrogation of NR2E3 homodimerization (one order of magnitude less than the wild-type protein).

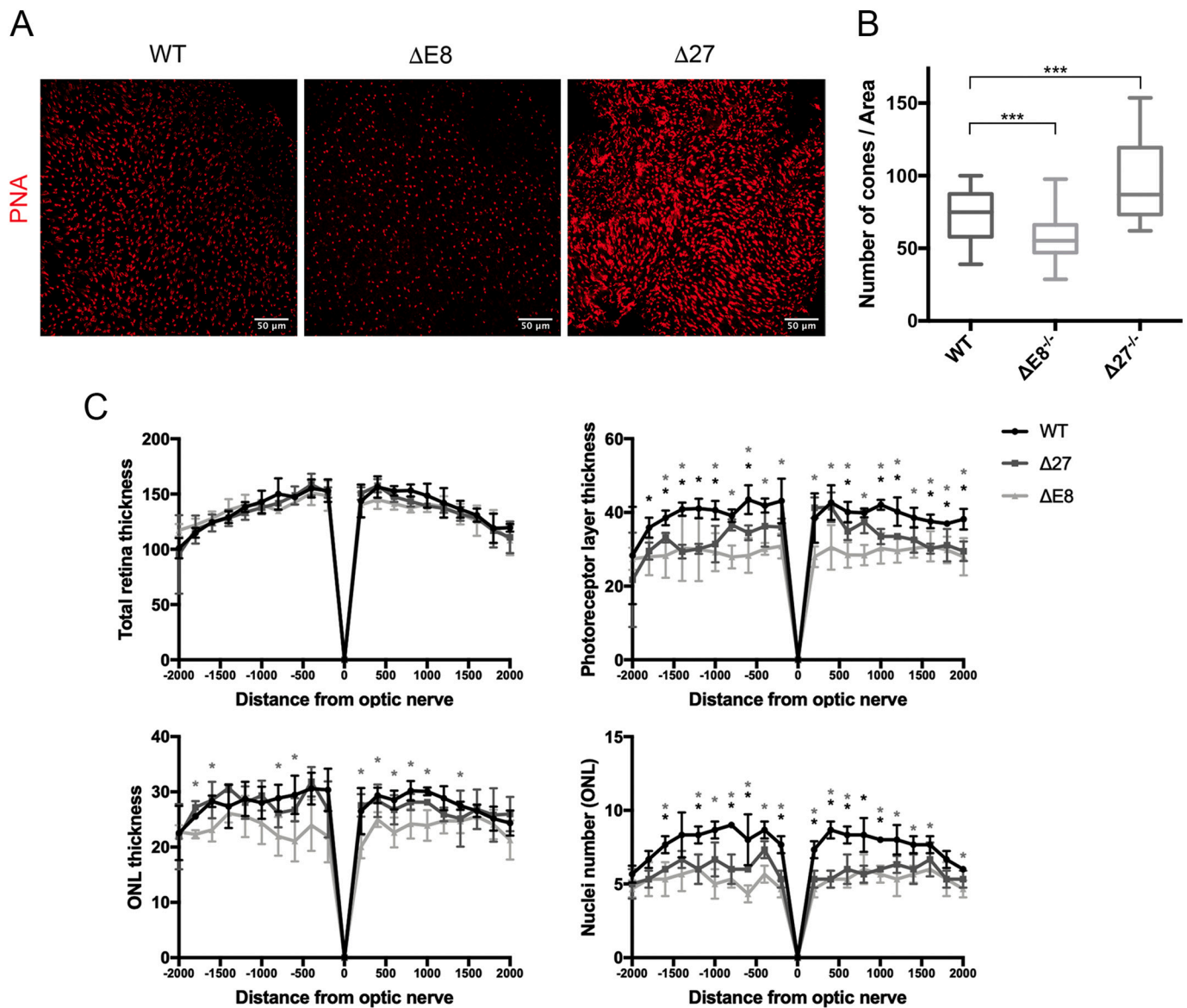
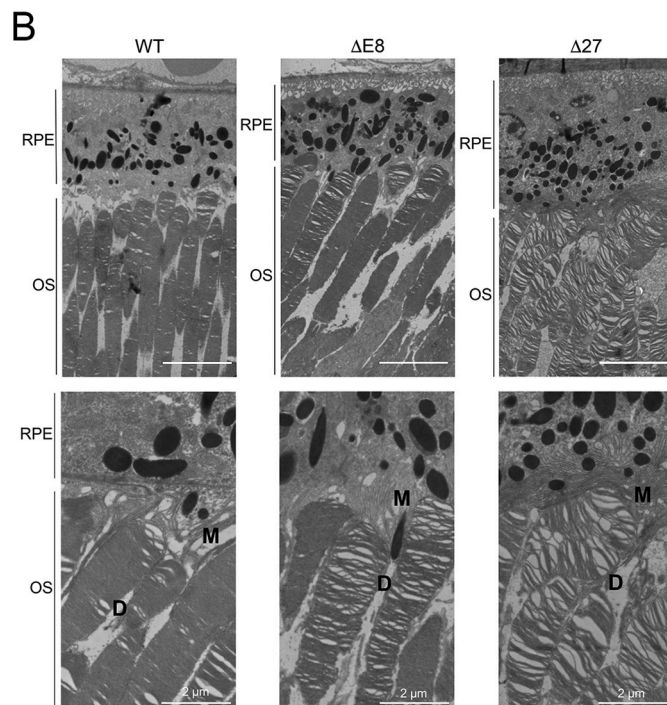
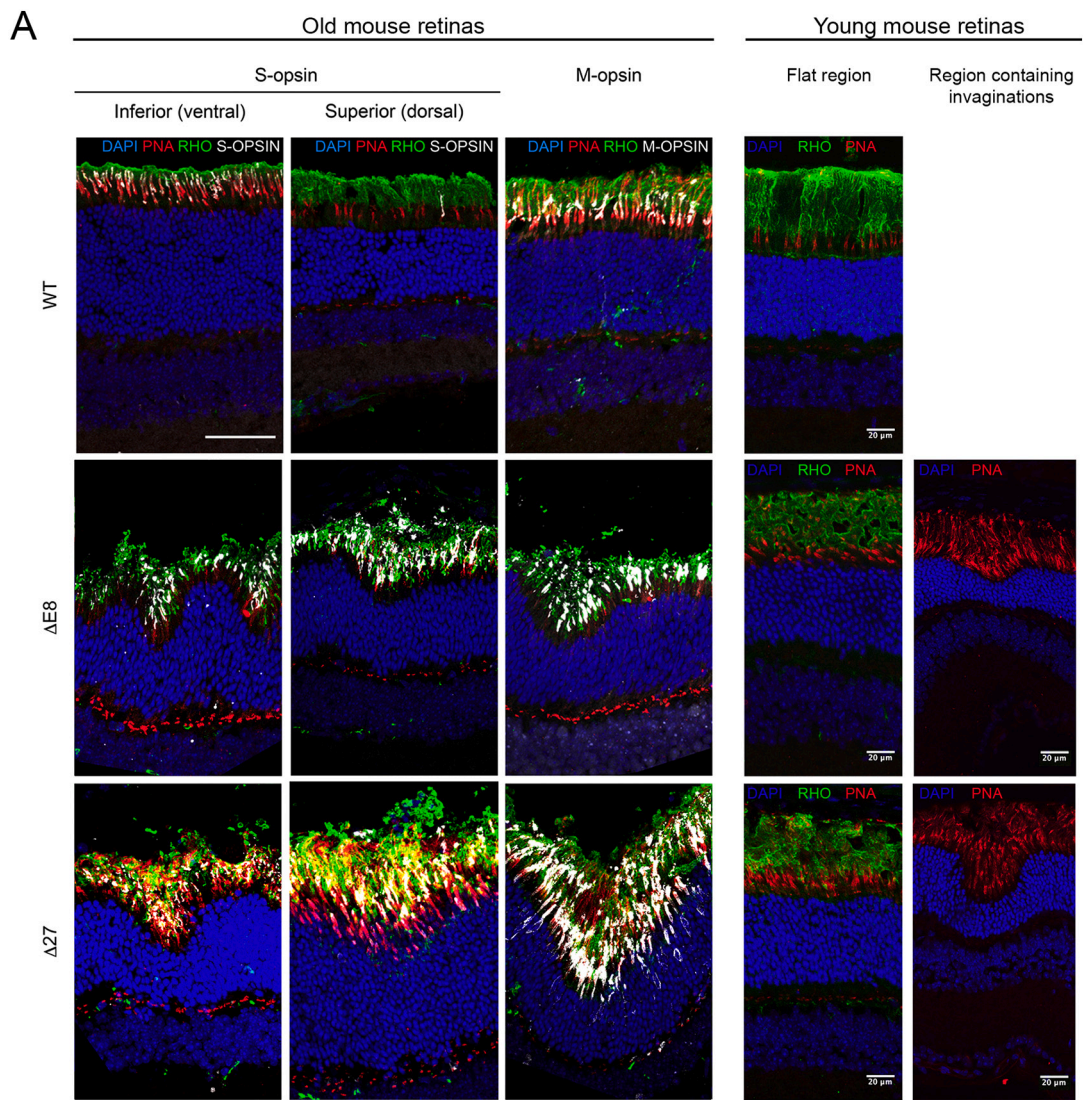


**Fig. 3.** Altered number of cones and decreased number of photoreceptor nuclei in the two *Nr2e3* mutants generated by gene-editing compared to controls. **A)** Whole mount retinas from  $\Delta E8$  homozygous mice show a consistent reduction in the number of cones whereas those from  $\Delta 27$  homozygous mice display a higher number of cones compared to wild-type mouse retinas. Representative images. Cones are labelled with PNA (red). **B)** Quantification of cone number showed statistically significant differences between the wildtype and homozygote retinas from the two mouse models. Mean values and standard deviation from 10 to 12 independent measurements in three animals per genotype were obtained and analyzed (Two-way ANOVA test, \*\*\*  $p < 0.001$ ). The  $\Delta E8$  mutant (low levels of truncated NR2E3 protein lacking dimerization and repressor domains) shows decreased levels of total cone photoreceptors, whereas the  $\Delta 27$  mutant (normal levels of a mutant NR2E3 protein that cannot dimerize) show increased levels of total cone photoreceptors. **C)** Morphometric measurements in semi-thin retinal sections containing the optic nerve show thinning of the photoreceptor layer, outer nuclear layer and number of nuclei row in mutant *Nr2e3* mice. Measurements were taken at 200  $\mu$ m intervals, and mean values and standard deviation were obtained from three animals per genotype. For statistical analysis, Mann-Whitney test was performed (\*  $p < 0.05$ ). Both  $\Delta E8$  and  $\Delta 27$  mutants showed a thinner photoreceptor layer and a clear reduction of the nuclei row number of the ONL. Besides, the ONL of  $\Delta E8$  homozygous mutant mice (but not that of  $\Delta 27$  mutants) was also statistically significantly thinner. (For interpretation of the references to colour in this figure legend, the reader is referred to the web version of this article.)

*NR2E3* mutations. The  $\Delta E8$  phenotype might be comparable to that shown by RP, with progressive degeneration of rods and subsequent involvement of cones. The  $\Delta 27$  resemble the phenotype of ESCS, with an overabundance of cones and a reduced number of dysfunctional rods.

Morphometric analysis of retinal sections, which include cell number and thickness measurements of different layers, has been used in examining retinal diseases. Measurements from blue stained semi-thin sections of adult retinas at the optic nerve level were used for morphometric analysis to quantify the morphological differences observed in the ultrastructural analysis ( $n = 3$ ). No clear differences in the

total retina thickness were detected comparing the wild type and the mutant retinas. However, the thickness of the photoreceptor layer (PL) is decreased in both  $\Delta E8$  and  $\Delta 27$  mutants, although this reduction is more evident in the  $\Delta E8$  than in the  $\Delta 27$  mutant (Fig. 3C, upper panels).  $\Delta E8$  mutants also showed a reduction in the ONL thickness, which is not observed in the  $\Delta 27$  mutants. Even so, both mutants show a significant decrease in the number of nuclei present in the ONL, comparable to the decrease observed in the *rd7* mutant (Webber et al., 2008). The decline in the number of nuclei is more notable in the  $\Delta E8$  than in the  $\Delta 27$  mutant, pointing to a progressive degeneration of the retina in the  $\Delta E8$  mutant (Fig. 3C, lower panels).



(caption on next page)

**Fig. 4.** Phenotypic alterations in the retinas of the two *Nr2e3* mouse mutants include cone-rich invaginations and photoreceptor disk abnormalities. A) Immunohistochemical characterization of wild type,  $\Delta E8$  and  $\Delta 27$  mutant retinas in old (> 12 months) and young (p60) mice. Retinal sections were stained to all types of cones (PNA, red), rods (anti-Rho, green), and cones expressing S- or M-opsins (white). Invaginations containing rods as well as M- and S-cones were detected in  $\Delta 27$  and  $\Delta E8$  homozygote retinas. The larger number of cones is particularly evident in the  $\Delta 27$  retinas. Nuclei are counter stained with DAPI (blue). Scale bar: 50  $\mu\text{m}$  (left) and 20  $\mu\text{m}$  (right). B) Ultrastructural images obtained by transmission electron microscopy (TEM) of wild type and mutant retinas, focusing on photoreceptors. A magnification of the outer segment of photoreceptors is displayed below, showing disarranged membranous disk stacks (D) in the two mutants, and longer microvilli (M) in the  $\Delta 27$  samples. Retinal layers are indicated as follows: retinal pigment epithelium (RPE), outer segment (OS), inner segment (IS) and outer nuclear layer (ONL). Scale bar: 5  $\mu\text{m}$  (top) and 2  $\mu\text{m}$  (bottom). (For interpretation of the references to colour in this figure legend, the reader is referred to the web version of this article.)

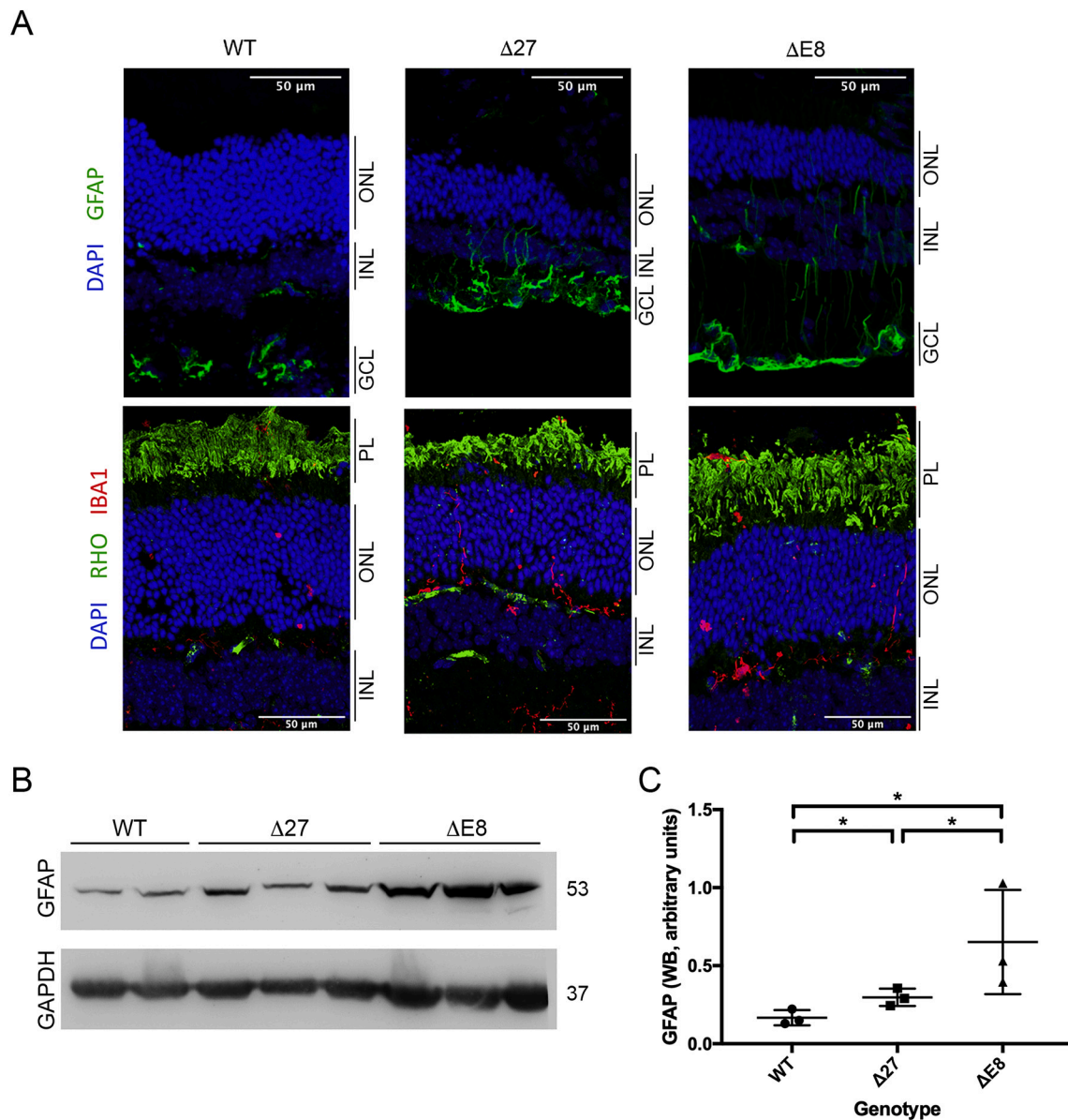
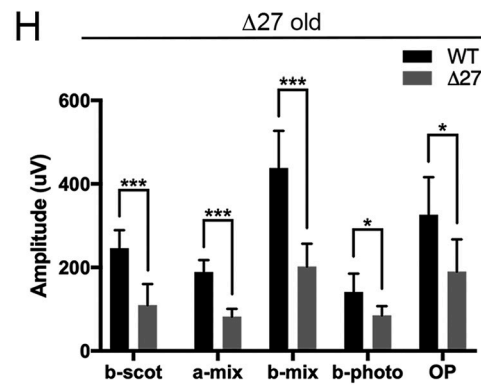
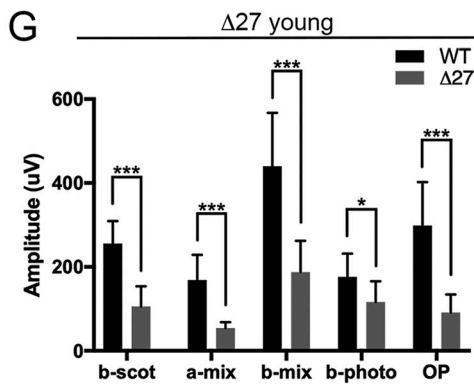
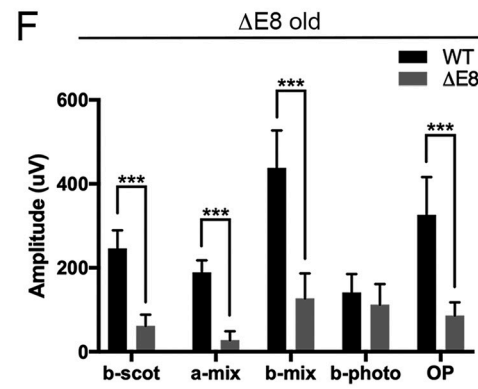
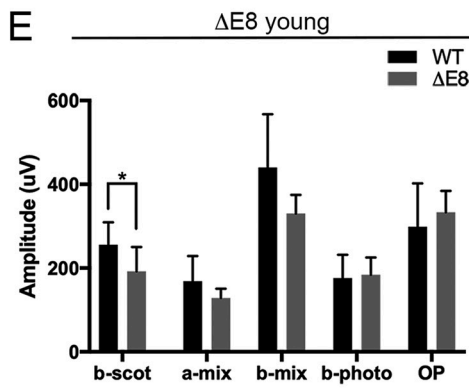
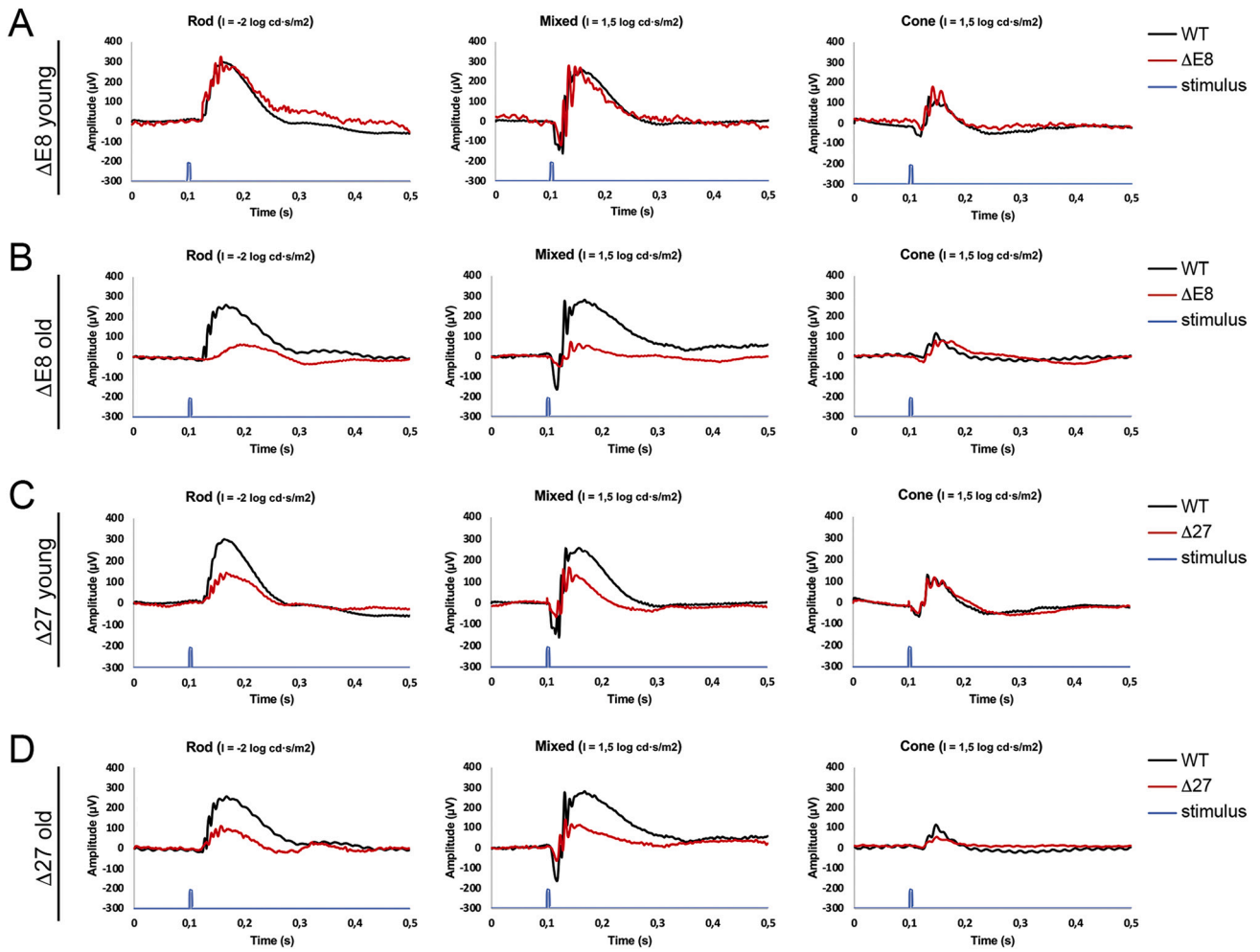


**Fig. 5.** The two mutant *Nr2e3* models show an increased expression of glial markers indicative of retinal stress. A) Immunohistochemical staining of Müller cells and microglia cells in the retina. Top retinal sections were stained with anti-GFAP (mainly expressed in Müller cells, green), showing an increase in GFAP-positive columnar processes in the two mutant *Nr2e3* models. Bottom panels depict retinal sections stained for rods (Rho, green) and microglial marker (Iba1, red), showing microglia infiltration in synaptic plexiform layers and inner photoreceptor segment layer. Nuclei are counterstained with DAPI (blue). Retinal layers are indicated: photoreceptor layer (PL), outer nuclear layer (ONL), inner nuclear layer (INL) and ganglion cell layer (GCL). Scale bar: 50  $\mu\text{m}$ . B) Immunodetection of GFAP (53 kDa) in the wild type and mutant retinas, and C) quantification, which confirmed the statistically significant increase in GFAP-positive cells in both  $\Delta E8$  and  $\Delta 27$  mutant retinas, although the levels of GFAP are higher in the  $\Delta E8$  mutant. GAPDH (37 kDa) was used as a loading control. Bars represent data (Mean  $\pm$  SD) of GFAP expression (Mann-Whitney test, \*  $p < 0.05$ ). (For interpretation of the references to colour in this figure legend, the reader is referred to the web version of this article.)



(caption on next page)

**Fig. 6.** Electrophysiological recordings (ERGs) of *Nr2e3*  $\Delta E8$  and  $\Delta 27$  homozygous animals show differential functional alterations in the two mutants. Representative ERG recordings obtained from wild type (black line) and *Nr2e3* mutant (red line) retinas. The two *Nr2e3* mutants show distinct recordings, which confirm physiological differences in the affectation of rods and cones as well as in the progression with age, and also indicating that they are potential models for different human diseases caused by *NR2E3* mutations. A) ERG measurements in young *Nr2e3*  $\Delta E8$  mice (3–4 months) show an initial decrease in rods activity (b-scot) compared to age-matched controls ( $n = 5-8$  animals per group). B) Photoreceptor activity is clearly abrogated with age (7–12 months old), indicating a degenerative process. C) ERG measurements in young *Nr2e3*  $\Delta 27$  mice show already alteration in photoreceptor activity (a-mix), mostly in rods (b-scot) but not so much in cones (b-photo). D) Remarkably, these electrophysiological alterations are stable and do not increase with age, indicating developmental defects in the differentiation of photoreceptors. E-H) Histogram representation of the averaged ERG wave amplitude for the four animal groups: (E)  $\Delta E8$  young, (F)  $\Delta E8$  old, (G)  $\Delta 27$  young and (H)  $\Delta 27$  old. Amplitude of stimulus application is shown (for light stimuli details, see the Material and Methods section). Bars represent data (Mean  $\pm$  SD) of b-scot, a-mix, b-mix and b-photo from *Nr2e3*<sup>WT/WT</sup> (black bars) and *Nr2e3* mutant (grey bars) mice, as indicated. Statistically significant differences (T-student test) are indicated above the histogram bars (\*  $p < 0.05$ , \*\*  $p < 0.01$ , \*\*\*  $p < 0.001$ ). (For interpretation of the references to colour in this figure legend, the reader is referred to the web version of this article.)

### 3.4. Photoreceptor morphology and retinal layer structure are grossly altered in the homozygous mutant retinas

To study and compare the retinal layer structure and photoreceptor morphology in our mutant models, IHC staining was performed in young (p60) and old (> 12 months) wild type and mutant mice to ( $n = 3$ ). Although both  $\Delta E8$  and  $\Delta 27$  mutants display a retinal morphology with recognizable retinal layers, the structure of the layers was obviously altered in the mutants compared to the wild type retinas (Fig. 4A), although we could not observe structural differences between young and older individuals of the same genotype despite the different age. We could detect rhodopsin and cone opsin expression in the  $\Delta E8$  and the  $\Delta 27$  mutant retinas. The number of cones appears particularly increased in the retinas of the  $\Delta 27$  mice (Fig. 4A). Remarkably, regions with invaginations containing the three types of photoreceptors (rods and the two type of cones) were detected in the outer retina. The outer nuclear layer (ONL) was also altered in the two mutant retinas, with a lower number of nuclei rows in the invagination fold (Fig. 4A, left panels). These invaginations resemble the *rd7* rosettes (Cheng et al., 2011; Haider et al., 2001; Haider et al., 2006), which have been reported to contain an excess of cones (Haider et al., 2001), although in our mutants, the invaginations are shallower and mostly detected in the central retina (Supplementary Fig. 4). Concerning cone distribution, S-cones and M-cones are expected in opposite gradients across the wild type retina (Swaroop et al., 2010). Indeed, in wild type mouse, S-cones were present only in half of the retina. In contrast, in the  $\Delta 27$  mutant, whose number of cones was increased, S-cone expression was clearly detected throughout the whole retina without a gradient distribution (Supplementary Fig. 4).

Ultrastructural analysis of photoreceptors in mutant retinas also reveals alterations in the retinal layer structure and photoreceptor morphology. The photoreceptor layers (PL), spanning inner and outer segments (IS and OS, respectively), are thinner in the  $\Delta E8$  compared to the wildtype and  $\Delta 27$  individuals (Fig. 4B). Besides, the  $\Delta 27$  mutant presents affectation of the RPE microvilli, which apparently are more numerous than in the wild type (Fig. 4B). The  $\Delta E8$  as well as the  $\Delta 27$  mutants show structural problems in disk stacking in the photoreceptor outer segments, as the membranous disks are loosely packed compared to the wild type retinas (Fig. 4B).

### 3.5. Increased GFAP and *Iba1* levels are indicative of gliosis as a response to retinal stress in the homozygous mutant retinas

These results prompted us to analyze whether the retinal alteration at the plexiform layers in the mutants was associated to retinal stress. The retina undergoes a process of degeneration of photoreceptors in response to stress and glial cells play an important role in tissue maintenance. In retinal gliosis, Müller cells (retinal macroglia cells), astrocytes and microglia cells are activated and migrate upon conditions of high stress (Erickson et al., 1987; Gupta et al., 2003; Jones and Marc, 2005; Roesch et al., 2012). *Nr2e3* wild type and mutant retinas were stained with GFAP (expressed in Müller cells and astrocytes) and *Iba1* (expressed in microglia). In the marginal regions of the retina,  $\Delta E8$

and  $\Delta 27$  mutants show a clear increase in GFAP expression, with columnar staining (corresponding to Müller cells) and end-feet inter-digitation towards the photoreceptor layer (Fig. 5A top). Mutants also show *Iba1*-positive cells in the ONL, with an increase of microglial processes compared to the wild type, indicating stress and retinal degeneration (Fig. 5A bottom). To compare the damage between the wild type and mutant individuals ( $n \geq 3$ ), GFAP protein expression was quantified by western blotting (Fig. 5B).

Both mutants exhibit a significant increase in the GFAP expression compared to the wild type, as expected according to the immunostaining results. However, the  $\Delta E8$  mutant shows higher levels of GFAP compared to the  $\Delta 27$  mutant, indicating a more aggressive degenerative process, in accordance also with the lower number of photoreceptor nuclei observed (Fig. 5C).

To assess whether reduction in the PL and ONL was due to increased cell death, we performed detection of active caspase-3 and caspase-7 apoptosis markers (Supplementary Fig. 5). No differences were observed between the wild type and the mutant mice. These results were also confirmed by negative immunohistochemistry detection of cleaved caspase-3 (data not shown).

### 3.6. Retinal electrophysiology is differentially altered in the two *Nr2e3* mutant models

Visual function was assessed by electroretinography (ERG) waveforms obtained in wild type and each of the CRISPR-generated *Nr2e3* mutants at 3–4 months-old and 7–12 months-old animals (Fig. 6). The electrical response to light was recorded after overnight dark-adaptation to increasing light flashes in scotopic and photopic (b-scotopic, a-mixed, b-mixed and b-photopic) conditions. The amplitude of the scotopic b-wave (b-scotopic, b-scot) assess the functionality of the rod-driven circuitry. The a-wave amplitude in these conditions (a-mixed, a-mix) reflects the activity of both rod and cone photoreceptors, whereas the b-wave (b-mixed, b-mix) include synaptic cells. Photopic b-wave (b-photopic, b-photo) test the cone-driven circuitry under photopic conditions by measuring the response to intense flashes of light in the presence of rod-saturating light stimulation.

At 3–4 months (p90-120), the amplitude of the scotopic b-wave (b-scot) showed significant differences between wild type and  $\Delta E8$  mice, indicating alterations in the rod response. No significant differences were found in the a-mix, b-mix and b-photo (Fig. 6A and E). In contrast, at 7–12 months (p210-360), significant differences between wild type and  $\Delta E8$  mice were found when analyzing nearly all photoreceptors responses to light: in the b-scot, a-mix and b-mix recordings. However, the b-photo wave was not altered between the wild type and the  $\Delta E8$  individuals (Fig. 6B and F). The increase in the affectation of the b-scot in young compared to old mice and the posterior addition of significant differences in the photoreceptor and synaptic cells is highly indicative of a degenerative process. The initial affectation of rods followed by alterations in other cell types is comparable to the RP human phenotype.

Remarkably,  $\Delta 27$  mice showed significant differences in all of the parameters measured, b-scot, a-mix, b-mix and b-photo, at early

adulthood (3–4 months old, Fig. 6C and G). Electrophysiological alterations exhibited by the  $\Delta 27$  mutants are comparable to those found in the *rd7* mice (Akhmedov et al., 2000; Chakraborty et al., 2013; Ueno et al., 2005). The  $\Delta 27$  alterations were maintained and equivalent at initial and later stages (7–12 months old, Fig. 6D and H), thus indicating that the alterations were most probably produced by developmental defects, resembling the ESCS human phenotype, also in the evident affectation of rod function.

#### 4. Discussion

In humans, mutations in *NR2E3* result in functional changes in the encoded transcription factor that affect promoter target site binding, interaction with other partners, homodimerization, and regulation of transactivation/repression activity (Kanda and Swaroop, 2009; von Alpen et al., 2015), thereby altering the expression of downstream genes relevant for photoreceptor differentiation and leading to distinct retinopathies depending on the primarily affected type of photoreceptors.

RP occurs in the differentiated retina as a consequence of the progressive neurodegeneration of rod photoreceptors, whereas ESCS is caused by S-cone hypertrophy at expense of rod defective differentiation during retinal development (Coppieters et al., 2007; Escher et al., 2009; Favre, 1958; Gire et al., 2007; Haider et al., 2000; Schorderet and Escher, 2009).

We have generated different gene-edited alleles using CRISPR and the Cas9 D10A nickase variant. We opted for the nickase because we surmised that the use of two guides to produce a DSB in a precise target site, and thus, the requirement of four guides to achieve a deletion of a medium size fragment diminished the probability of off-target events. At least in our hands, the Cas9 nickase was effective in generating many different alleles, although with a clear preference for one of the main target sites (34% of the mice presented gene-edited alleles at the 5' position, with only 1,6% showing the designed deletion of the full exon 8) (Data in Brief, companion article).

Most genes generate multiple isoforms by mechanisms such as alternative splicing, intron retention and alternative transcription start/stop sites. These mechanisms are especially common in the central nervous system, which contains specific alternative splicing programs contributing to the complexity of neural function (Raj and Blencowe, 2015; Reyes and Huber, 2018; Taliaferro et al., 2016). Recently, a novel isoform of a retinal degeneration gene has been described to be the unique isoform expressed by photoreceptors (Ray et al., 2020), highlighting the importance of characterizing different gene isoforms in order to avoid misinterpretation of disease-linked mutations. In this study, we present a new shorter NR2E3 protein isoform, previously unreported in mice, generated by intron 7 retention. The production of this isoform appears to be developmentally regulated, since it is undetectable at E18 and its expression levels increase at P10, being higher at adult stages in wild-type retinas (Fig. 1E-G).

Considering that: i) this transcript isoform is present at least in human and mouse, ii) the evolutionary conservation of the in-frame stop codon at the beginning of the retained intron 7, iii) the identification of a putative ESE for intron 7 recognition, iv) the differential developmental transcription, and v) the detection of the shorter size protein, all these facts together are extremely suggestive of a physiological role, as yet undetermined, for this isoform. We believe that some of the phenotypic traits observed in our *Nr2e3* mutant mouse models might be caused by the production and/or misexpression of this isoform.

Our results suggest that the  $\Delta E8$  mutation, with the deletion of exon 8 including the 3'UTR, produces only the shorter size protein isoform. The phenotype of this mutant showed severe alterations in the maintenance and homeostasis of rod photoreceptors, with progressive rod cell death, similar to the human RP phenotype. The expression levels of the transcript and the protein do not fully correlate in this mutant. A plausible explanation is that the 3'UTR contains sequences that regulate mRNA stability and protein translation, and the deletion of these

sequences in the  $\Delta E8$  allele results in lower translation levels. Therefore, we cannot discard that the observed phenotype is due to either the absence of the full length NR2E3 protein displaying the dimerization and repressor domains, or the production of the short isoform, overall acting as a strong knockdown allele. On the other hand, the deleted region might contain cis-regulatory elements of flanking genes, which could contribute to the mutant phenotype. We deem this unlikely, as data from Topologically Associated Domain (TAD) chromatin architecture and ENCODE (identification of candidate cis-regulatory elements) do not support that deletion of exon 8 is altering chromatin structure, and the phenotype observed is restricted to the retina (Supplementary Fig. 6).

The  $\Delta E8$  mutant presents a lower number of nuclei, and thinner PL and ONL than the  $\Delta 27$  mutant (Fig. 3H), indicating a more severe degeneration. The differences in the degenerative process are also significant when analyzing the markers of retinal stress, GFAP and Iba1 (Fig. 5). However, we did not observe differences in the caspase-3 and caspase-7 apoptosis markers between the wild type and mutant retinas indicating degeneration is not caused by apoptosis (Supplementary Fig. 5), in accordance with studies in the *rd7* mouse model and the knockout in zebrafish, where TUNEL assays were not significant (Cheng et al., 2011; Xie et al., 2019). Aberrant photoreceptor structure and disk packaging (Fig. 4B) are very likely to alter the phototransduction pathway and affect the visual function, as shown in ERG records (Fig. 6). The initial reduction in rods (b-scot) and posterior affectation of photoreceptor and synaptic activity in the  $\Delta E8$  mice is consistent with the progressive retinal neurodegeneration phenotype and attrition of photoreceptor cells observed in retinal slides. The reduction in the b-scot is indicative of higher rod affectation, similarly to what occurs in RP human patients.

In contrast, the  $\Delta 27$  mutation clearly produces two proteins, the long isoform lacking the dimerization domain, and the short isoform. The production of these isoforms at opposite levels in different retinal developmental stages compared to the wild-type retinas may have an impact in the phenotype: at P10, when the expression of *Nr2e3* peaks and rods differentiate, the long isoform is barely produced and the short isoform is expressed at higher levels. In the adult, instead the expression of the long isoform is more than 2-fold that of the wild-type. The observed phenotype of the  $\Delta 27$  mutant could be the result of this overall differential long vs short isoform expression, plus the incapability of the long isoform to dimerize.

Overall, the phenotypic effects observed are compatible with the inability to repress cone genes, increasing the number of S-cones and causing a very similar phenotype to ESCS in humans. The  $\Delta 27$  homozygotes show electrophysiological alterations in photoreceptor and synaptic activity indicating development defects, consistent with the observed higher number of cones and severe alteration of rod function, resembling ESCS patient phenotype. In humans, ESCS-associated mutations in exon 8 of *NR2E3* are also associated to a milder retinal degeneration (Audo et al., 2008). Note that although rhodopsin was detected in our mutant retinal sections, it may not indicate the presence of fully differentiated rods. A hybrid type of photoreceptor expressing both rod and cone genes has been reported in the *rd7* mouse (Corbo and Cepko, 2005). Besides, some authors have also reported a rod/cone intermediate population: such “cods” have been recently characterized in retinal organoids from a NRL null patient showing an ESCS phenotype (Kallman et al., 2020). Reported mutations (mainly missense) in *NR2E3* causing ESCS follow an autosomal recessive inheritance. The c.1101-1G > A human mutation (all reported human mutations in exon 8 are in Supplementary Table 1) is a splice acceptor mutation in intron 7, which has been reported to cause ESCS in homozygosis. If intron 7 is retained, we would expect a higher expression of the short isoform. Further functional tests are necessary to evaluate the pathogenic potential of the long vs short isoform misregulation, which could shed light on the mechanisms underlying *Nr2e3* mutations heterogeneity.

**Table 1**  
Functional effect of NR2E3 mutations in exon 8 in human and mouse.

Human patients				
DNA change	Protein change	Affected region	Predicted effect/functional characterization	References
c.1120C > T	p.L374F	LBD/H10	Impaired dimerization	(Cima et al., 2012)
c.1154G > C	p.R385P	LBD/ H10	Impaired dimerization Decreased protein expression Affected interaction with NRL and NR1D1	(Haider et al., 2000; Kanda and Swaroop, 2009; von Alpen et al., 2015)
c.1217A > G	p.D406G	LBD/AF2	Potentiated activator function	(Manayath et al., 2014)
c.1220T > A	p.M407K	LBD/ AF2	Impaired dimerization Normal levels of activation and repression	(Haider et al., 2000; Kanda and Swaroop, 2009; von Alpen et al., 2015)
Mouse models				
Mutation	Predicted effect	Human disease	Phenotype	References
$\Delta$ exons1-6 <i>rd7</i>	No protein No protein	ESCS-like ESCS-like	$\uparrow$ cone genes, $\downarrow$ nuclei (ONL), presence of rosettes $\downarrow$ rod genes (p2-p10) $\uparrow$ cone genes, $\downarrow$ nuclei (ONL), presence of rosettes, altered ERGs (p180)	(Webber et al., 2008) (Akhmedov et al., 2000a; Cheng et al., 2011; Haider et al., 2001; Webber et al., 2008) This article
$\Delta$ 27	9 aa in-frame deletion (dimerization domain)	ESCS-like	$\downarrow$ homodimerization, $\uparrow$ cone number, presence of retinal invaginations, $\downarrow$ nuclei (ONL), altered ERGs (p90)	This article
$\Delta$ 88	Dimerization and repressor domain deletion	RP-like	$\downarrow$ homodimerization, $\downarrow$ cone number, presence of retinal invaginations, $\downarrow$ nuclei (ONL), altered ERGs (p360)	This article

LBD: Ligand binding domain; H10: helix 10 (dimerization domain); AF2: activation-function-2 (repressor domain), *rd7*: retinal degeneration 7; L1: Line-1; ESCS: Enhanced S-cone Syndrome; RP: Retinitis Pigmentosa; ONL: Outer Nuclear Layer; ERG: Electroretinography.

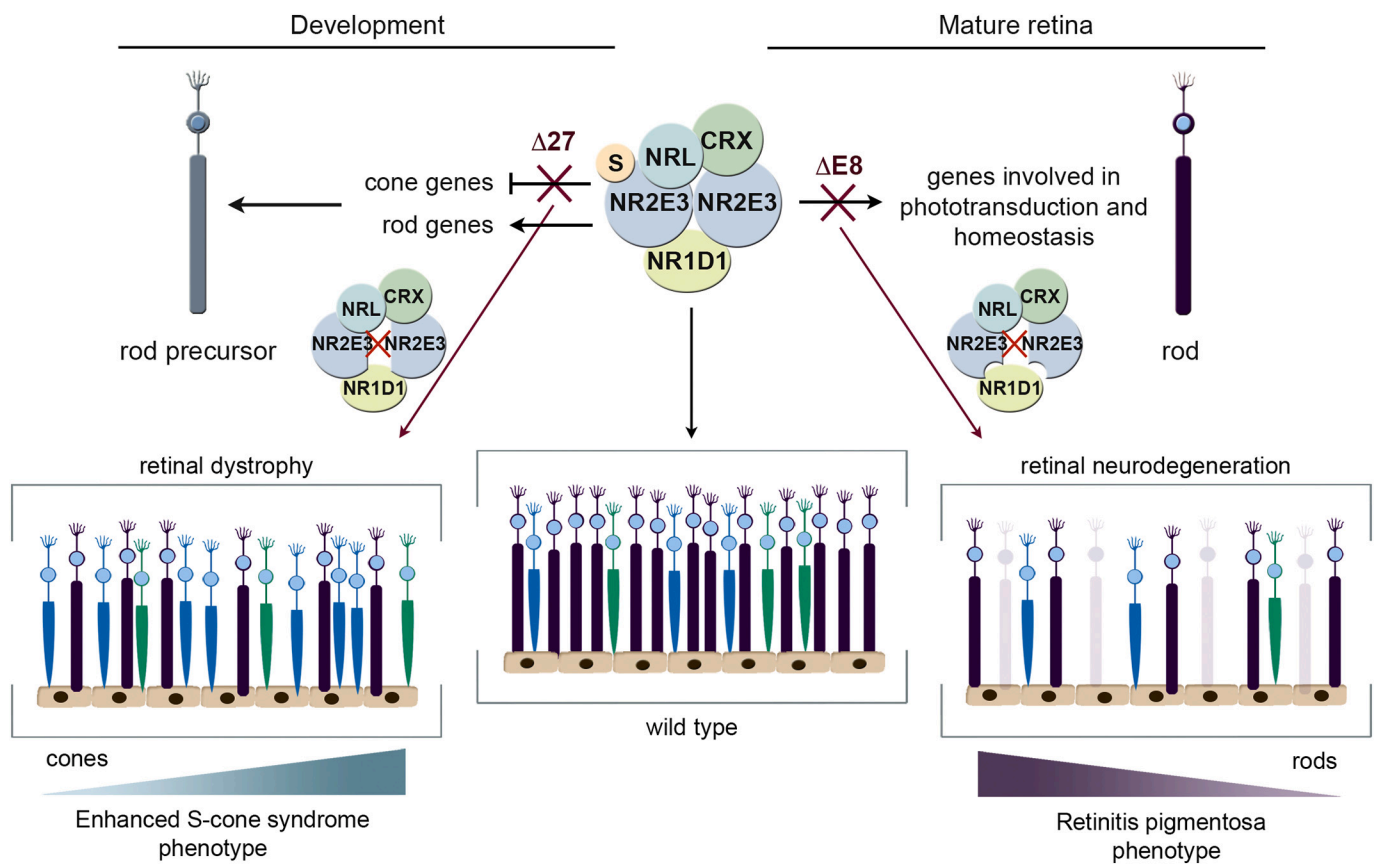


**Fig. 7.** Modeling *NR2E3*-retinal dystrophies in mouse to generate mutants resembling the enhanced S-cone syndrome (ECS) and retinitis pigmentosa (RP) human phenotypes. *NR2E3* is necessary for inhibition of cone genes (default pathway) and activation of rod differentiation genes in retinal precursors during retinal development, but it is also relevant for rod functional maintenance and survival. S indicates reversible SUMO modification of *NR2E3*, since sumoylation is required for cone gene repression (Onishi et al., 2009). Mutations that affect homeostasis of rod photoreceptors would cause RP, while mutations affecting repression of S-cone genes would cause ECS. The  $\Delta 27$  mutant encodes a dimerization incompetent variant of *NR2E3*, failing to repress cone genes leading to increased number of dysfunctional cones, triggering initial death of rods, and causing an ECS-like phenotype, mostly reflecting a gain-of-function effect. The  $\Delta E8$  mutant lacks the dimerization and repression domains and only expresses the short isoform of *NR2E3* at low levels, failing to maintain the homeostasis of mature rods, probably reflecting a loss-of-function effect, thus leading to a slow and progressive attrition of rods and also cones with age, and showing a phenotype similar to the RP patients.

Homodimerization is impaired in both  $\Delta E8$  and  $\Delta 27$  mutants to the same extent (Fig. 2B), which means that the partial and complete deletion of exon 8 disrupt similarly the dimer formation. Therefore, the 9 amino acids deleted in the  $\Delta 27$  mutant are essential for homodimer formation and confirm the involvement of the alpha-helix H10 as the main dimerization domain. Although most nuclear orphan receptors act as homodimers, some function might be exerted by *NR2E3* monomers binding to its recognized motifs, thus explaining why the phenotype of both mutants is different. In fact, some authors had previously reported that the dimerization potential of *NR2E3* did not necessarily correlate with transcriptional activity of *NR2E3* on rhodopsin and M-opsin promoters (von Alpen et al., 2015). In this context, comparison with the location and effect of patient mutations in the human ortholog gene can also shed light on the physiological role of *NR2E3* (Table 1).

The p.R385P and p.M407K mutations, respectively located in the H10 and AF2 domains (Table 1), result in a dimerization incompetent protein but still able to activate and repress within a normal range (von Alpen et al., 2015). These findings strongly suggest that dimerization is not essential for the *NR2E3* role as activator and/or repressor since the transcription factor would still retain the ability to bind DNA as a monomer. This hypothesis is supported by the fact that mutations located outside the dimer interface also cause typical ECSC, indicating that other factors, such as binding and recruitment of co-repressors, might be also altered mechanisms in disease.

Notably, whole mount retinas of  $\Delta 27$  mice show structures compatible with double or triple cones (Fig. 3C-G). Double cones have been

observed in many fish, birds, amphibians and reptiles (Ali and Anctil, 1976; Ebrey and Koutalos, 2001; Walls, 1943), but have never been described in the mammal retina. In both mouse and zebrafish, RPCs undergo symmetric terminal divisions to generate cones (Cepko, 2015; Suzuki et al., 2013; Turner et al., 1990). We cannot discard the possibility that the double cones observed in the  $\Delta 27$  retinas reflect a developmental defect in the terminal division of progenitor cells, which fail to produce two separated cones. Further work should clarify this differential trait. On the other hand, the increase number of cones observed in the  $\Delta 27$  retinas, also increase the chances of finding groups of double and triple cones.

Besides, the ONL and PL in the two mutants present cone-rich invaginations (Fig. 4A) similar to the rosettes detected in the *rd7* mouse retina (Cheng et al., 2011; Haider et al., 2001; Haider et al., 2006), although in our models we have not observed whorls, and the rich-cone invaginations are less profound and cluster in the central retina. Since one of the functions of *NR2E3* is the suppression of cone generation to prevent cone overpopulation of the retina (Haider et al., 2006), differences in the activation or repression of *NR2E3*-controlled genes may affect the spatial arrangement of photoreceptor cells.

In summary, we have identified two different protein isoforms produced by the *Nr2e3* gene, and generated two mouse models by deleting different domains encoded in the last *Nr2e3* exon, leading to two models of different human retinal dystrophies, RP and ECSC (Fig. 7). The *Nr2e3*  $\Delta E8$  mouse model expresses only the short isoform of *NR2E3*

and show progressive rod degeneration in aged animals, which causes high levels of stress and inflammation and eventually leads to the affection of remaining retinal cells. The *Nr2e3*  $\Delta 27$  mouse model expresses both isoforms, but none can dimerize. Cone genes cannot be repressed, which results in an increase in the number of S-cones and the consequent decrease in the number of rods, thus affecting retinal function. Our *Nr2e3*  $\Delta E8$  model is the first mouse model of RP caused by mutations in *Nr2e3*, whereas the *Nr2e3*  $\Delta 27$  model concurs with the *rd7* and knockout mouse models and resembles the ESCS human phenotype (Akhmedov et al., 2000; Chen et al., 2006; Haider et al., 2001; Webber et al., 2008).

Recent studies propose *Nr2e3* as a genetic modifier and broad-spectrum therapeutic agent to treat multiple forms of RP (Li et al., 2020). In this context, our models provide a valuable tool in studying *NR2E3*-caused diseases and allow us to comprehend molecular mechanisms of disease by dissecting genetic pathways and evaluate therapeutics.

## Funding

This research was supported by grants SAF2013-49069-C2-1-R, SAF2016-80937-R (Ministerio de Economía y Competitividad/FEDER), ACCI 2015 and ACCI 2016 (CIBERER /ISCIII) and 2017 SGR 738 (Generalitat de Catalunya) to GM; La Marató TV3 (Project Marató 201417-30-31-32); and the Instituto de Salud Carlos III, cofounded with the European Regional Development Fund (ERDF) within the “Plan Estatal de Investigación Científica y Técnica y de Innovación 2017–2020” (RD16/0008/0020; FIS/PI 18–00754) to PdIV. IAM is a fellow of the APIF-2019 (Universitat de Barcelona).

## Declaration of Competing Interest

The authors declare that they have no conflict of interest.

## Acknowledgements

The authors also acknowledge the technical support of Elena Laplaza and Laura Jiménez.

## Appendix A. Supplementary data

Supplementary data to this article can be found online at <https://doi.org/10.1016/j.nbd.2020.105122>.

## References

- Aísa-Marín, I., López-Iniesta, M.J., Marfany, G., 2020. Data on the Generation of Two *Nr2e3* Mouse Models by CRISPR/Cas9 D10A. Data in Brief, Companion Article. (in press).
- Akhmedov, N.B., Piriev, N.I., Chang, B., Rapoport, A.L., Hawes, N.L., Nishina, P.M., Nusinowitz, S., Heckenlively, J.R., Roderick, T.H., Kozak, C.A., Danciger, M., Davison, M.T., Farber, D.B., 2000. A deletion in a photoreceptor-specific nuclear receptor mRNA causes retinal degeneration in the *rd7* mouse. *Proc. Natl. Acad. Sci. U. S. A.* 97, 5551–5556. <https://doi.org/10.1073/pnas.97.10.5551>.
- Ali, M.A., Ancil, M., 1976. Retinas of fishes. *An Atlas*. <https://doi.org/10.1007/978-3-642-66435-9>.
- Audo, I., Michaelides, M., Robson, A.G., Hawlina, M., Vaclavik, V., Sandbach, J.M., Neveu, M.M., Hogg, C.R., Hunt, D.M., Moore, A.T., Bird, A.C., Webster, A.R., Holder, G.E., 2008. Phenotypic variation in enhanced S-cone syndrome. *Invest. Ophthalmol. Vis. Sci.* 49, 2082–2093. <https://doi.org/10.1167/iovs.05-1629>.
- Bernal, S., Solans, T., Gamundi, M.J., Hernan, I., De Jorge, L., Carballo, M., Navarro, R., Tizzano, E., Ayuso, C., Baiget, M., 2008. Analysis of the involvement of the *NR2E3* gene in autosomal recessive retinal dystrophies. *Clin. Genet.* 73, 360–366. <https://doi.org/10.1111/j.1399-0004.2008.00963.x>.
- Cartegni, L., Wang, J., Zhu, Z., Zhang, M.Q., Krainer, A.R., 2003. ESE finder: a web resource to identify exonic splicing enhancers. *Nucleic Acids Res.* 31, 3568–3571. <https://doi.org/10.1093/nar/gkg616>.
- Cepko, C.L., 2015. The determination of rod and cone photoreceptor fate. *Ann. Rev. Vis. Sci.* 21, 211–234. <https://doi.org/10.1146/annurev-vision-090814-121657>.
- Chakraborty, D., Conley, S.M., Naash, M.I., 2013. Overexpression of retinal degeneration slow (RDS) protein adversely affects rods in the *rd7* model of enhanced S-cone syndrome. *PLoS One* 8, 63321. <https://doi.org/10.1371/journal.pone.0063321>.
- Chen, S., Wang, Q.-L., Nie, Z., Sun, H., Lennon, G., Copeland, N.G., Gilbert, D.J., Jenkins, N.A., Zack, D.J., 1997. *Crx*, a novel *Otx*-like paired-homeodomain protein, binds to and transactivates photoreceptor cell-specific genes. *Neuron* 19, 1017–1030. [https://doi.org/10.1016/S0896-6273\(00\)80394-3](https://doi.org/10.1016/S0896-6273(00)80394-3).
- Chen, J., Rattner, A., Nathans, J., 2005. The Rod Photoreceptor-Specific Nuclear Receptor *Nr2e3* Represses Transcription of Multiple Cone-Specific Genes. <https://doi.org/10.1523/JNEUROSCI.3571-04.2005>.
- Chen, J., Rattner, A., Nathans, J., 2006. Effects of L1 retrotransposon insertion on transcript processing, localization and accumulation: lessons from the retinal degeneration 7 mouse and implications for the genomic ecology of L1 elements. *Hum. Mol. Genet.* 15, 2146–2156. <https://doi.org/10.1093/hmg/ddl138>.
- Cheng, H., Khanna, H., Oh, E.C.T., Hicks, D., Mitton, K.P., Swaroop, A., 2004. Photoreceptor-specific nuclear receptor *NR2E3* functions as a transcriptional activator in rod photoreceptors. *Hum. Mol. Genet.* 13, 1563–1575. <https://doi.org/10.1093/hmg/ddh173>.
- Cheng, H., Aleman, T.S., Cideciyan, A.V., Khanna, R., Jacobson, S.G., Swaroop, A., 2006. In vivo function of the orphan nuclear receptor *NR2E3* in establishing photoreceptor identity during mammalian retinal development. *Hum. Mol. Genet.* 15, 2588–2602. <https://doi.org/10.1093/hmg/ddl185>.
- Cheng, H., Khan, N.W., Roger, J.E., Swaroop, A., 2011. Excess cones in the retinal degeneration *rd7* mouse, caused by the loss of function of orphan nuclear receptor *Nr2e3*, originate from early-born photoreceptor precursors. *Hum. Mol. Genet.* 20, 4102–4115. <https://doi.org/10.1093/hmg/ddr334>.
- Cima, I., Brecej, J., Sustar, M., Coppieters, F., Leroy, B.P., De Baere, E., Hawlina, M., 2012. Enhanced S-cone syndrome with preserved macular structure and severely depressed retinal function. *Doc. Ophthalmol.* 125, 161–168. <https://doi.org/10.1007/s10633-012-9337-y>.
- Ciruela, F., Fernández-Dueñas, V., 2015. GPCR oligomerization analysis by means of BRET and dFRAP. In: Prazeres, D.M.F., Martins, S.A.M. (Eds.), *G Protein-Coupled Receptor Screening Assays: Methods and Protocols*. Springer New York, New York, NY, pp. 133–141. [https://doi.org/10.1007/978-1-4939-2336-6\\_10](https://doi.org/10.1007/978-1-4939-2336-6_10).
- Coppieters, F., Leroy, B.P., Beysen, D., Hellemans, J., De Bosscher, K., Haegeman, G., Robberecht, K., Wuyts, W., Coucke, P.J., De Baere, E., 2007. Recurrent mutation in the first zinc finger of the orphan nuclear receptor *NR2E3* causes autosomal dominant retinitis pigmentosa. *Am. J. Hum. Genet.* 81, 147–157. <https://doi.org/10.1086/518426>.
- Corbo, J.C., Cepko, C.L., 2005. A hybrid photoreceptor expressing both rod and cone genes in a mouse model of enhanced S-cone syndrome. *PLoS Genet.* 1, e11. <https://doi.org/10.1371/journal.pgen.0010011>.
- Ebrey, T., Koultalos, Y., 2001. Vertebrate photoreceptors. *Prog. Retin. Eye Res.* [https://doi.org/10.1016/S1350-9462\(00\)00014-8](https://doi.org/10.1016/S1350-9462(00)00014-8).
- Erickson, P.A., Fisher, S.K., Guerin, C.J., Anderson, D.H., Kaska, D.D., 1987. Glial fibrillary acidic protein increases in Müller cells after retinal detachment. *Exp. Eye Res.* 44, 37–48.
- Escher, P., Gouras, P., Roduit, R., Tiab, L., Bolay, S., Chen, S., Tsai, C., Hayashi, M., Zernant, J., Merriam, E., Mermod, N., Allikmets, R., Munier, F.L., Daniel, F., 2009. Mutations in *NR2E3* can cause dominant or recessive retinal degenerations in a same family. *Hum. Mutat.* 30, 342–351. <https://doi.org/10.1002/humu.20858>.
- Favre, M., 1958. Two cases of hyaloid-retinal degeneration. *Ophthalmologica* 135, 604–609. <https://doi.org/10.1159/000303360>.
- Freund, C.L., Gregory-Evans, C.Y., Furukawa, T., Papaioannou, M., Looser, J., Ploder, L., Bellingham, J., Ng, D., Herbrick, J.-A.S., Duncan, A., Scherer, S.W., Tsui, L.-C., Loutradis-Anagnostou, A., Jacobson, S.G., Cepko, C.L., Bhattacharya, S.S., McInnes, R.R., 1997. Cone-rod dystrophy due to mutations in a novel photoreceptor-specific homeobox gene (*CRX*) essential for maintenance of the photoreceptor. *Cell* 91, 543–553. [https://doi.org/10.1016/S0092-8674\(00\)80440-7](https://doi.org/10.1016/S0092-8674(00)80440-7).
- Furukawa, T., Morrow, E.M., Cepko, C.L., 1997. *Crx*, a novel *otx*-like homeobox gene, shows photoreceptor-specific expression and regulates photoreceptor differentiation. *Cell* 91, 531–541. [https://doi.org/10.1016/S0092-8674\(00\)80439-0](https://doi.org/10.1016/S0092-8674(00)80439-0).
- Gire, A.I., Sullivan, L.S., Bowne, S.J., Birch, D.G., Hughbanks-Wheaton, D., John, R., Daiger, S.P., 2007. The Gly56Arg mutation in *NR2E3* accounts for 1-2% of autosomal dominant retinitis pigmentosa. *Mol. Vis.* 13, 1970–1975.
- Gupta, N., Brown, K.E., Milam, A.H., 2003. Activated microglia in human retinitis pigmentosa, late-onset retinal degeneration, and age-related macular degeneration. *Exp. Eye Res.* 76, 463–471. [https://doi.org/10.1016/S0014-4835\(02\)00332-9](https://doi.org/10.1016/S0014-4835(02)00332-9).
- Haider, N.B., Jacobson, S.G., Cideciyan, A.V., Swiderski, R., Streb, L.M., Searby, C., Beck, G., Hockey, R., Hanna, D.B., Gorman, S., Duhl, D., Carmi, R., Bennett, J., Weleber, R.G., Fishman, G.A., Wright, A.F., Stone, E.M., Sheffield, V.C., 2000. Mutation of a nuclear receptor gene, *NR2E3*, causes enhanced S cone syndrome, a disorder of retinal cell fate. *Nat. Genet.* 24, 127–131. <https://doi.org/10.1038/72777>.
- Haider, N.B., Naggert, J.K., Nishina, P.M., 2001. Excess cone cell proliferation due to lack of a functional *NR2E3* causes retinal dysplasia and degeneration in *rd7/rd7* mice. *Hum. Mol. Genet.* 10, 1619–1626. <https://doi.org/10.1093/hmg/10.16.1619>.
- Haider, N.B., DeMarco, P., Nystuen, A.M., Huang, X., Smith, R.S., McCall, M.A., Naggert, J.K., Nishina, P.M., 2006. The transcription factor *Nr2e3* functions in retinal progenitors to suppress cone cell generation. *Vis. Neurosci.* 23, 917–929. <https://doi.org/10.1017/S095252380623027X>.
- Human Gene Mutation Database (HGMD), 2017. <https://hgmd.cf.ac.uk> (accessed 7.30.20).
- Jones, B.W., Marc, R.E., 2005. Retinal remodeling during retinal degeneration. *Exp. Eye Res.* 81, 123–137. <https://doi.org/10.1016/j.exer.2005.03.006>.
- Kallman, A., Capowski, E.E., Wang, J., Kaushik, A.M., Jansen, A.D., Edwards, K.L., Chen, L., Berlinicke, C.A., Joseph Phillips, M., Pierce, E.A., Qian, J., Wang, T.H., Gamm, D.M., Zack, D.J., 2020. Investigating cone photoreceptor development using patient-derived *NRL* null retinal organoids. *Commun. Biol.* 3, 82. <https://doi.org/10.1038/>

- s42003-020-0808-5.
- Kanda, A., Swaroop, A., 2009. A comprehensive analysis of sequence variants and putative disease-causing mutations in photoreceptor-specific nuclear receptor NR2E3. *Mol. Vis.* 15, 2174–2184.
- Kobayashi, M., Takezawa, S.I., Hara, K., Yu, R.T., Umesono, Y., Agata, K., Taniwaki, M., Yasuda, K., Umesono, K., 1999. Identification of a photoreceptor cell-specific nuclear receptor. *Proc. Natl. Acad. Sci. U. S. A.* 96, 4814–4819. <https://doi.org/10.1073/pnas.96.9.4814>.
- Li, S., Datta, S., Brabbit, E., Love, Z., Woytowicz, V., Flattery, K., Capri, J., Yao, K., Wu, S., Imboden, M., Upadhyay, A., Arumugham, R., Thoreson, W.B., DeAngelis, M.M., Haider, N.B., 2020. *Nr2e3* is a genetic modifier that rescues retinal degeneration and promotes homeostasis in multiple models of retinitis pigmentosa. *Gene Ther.* <https://doi.org/10.1038/s41434-020-0134-z>.
- Manayath, G.J., Namburi, P., Periasamy, S., Kale, J.A., Narendran, V., Ganesh, A., 2014. A novel mutation in the *NR2E3* gene associated with Goldmann-Favre syndrome and vasoproliferative tumor of the retina. *Mol. Vis.* 20, 724–731.
- Mears, A.J., Kondo, M., Swain, P.K., Takada, Y., Bush, R.A., Saunders, T.L., Sieving, P.A., Swaroop, A., 2001. *Nrl* is required for rod photoreceptor development. *Nat. Genet.* 29, 447–452. <https://doi.org/10.1038/ng774>.
- Milam, A.H., Rose, L., Cideciyan, A.V., Barakat, M.R., Tang, W.X., Gupta, N., Aleman, T.S., Wright, A.F., Stone, E.M., Sheffield, V.C., Jacobson, S.G., 2002. The nuclear receptor NR2E3 plays a role in human retinal photoreceptor differentiation and degeneration. *Proc. Natl. Acad. Sci. U. S. A.* 99, 473–478. <https://doi.org/10.1073/pnas.022533099>.
- Mitton, K.P., Swain, P.K., Chen, S., Xu, S., Zack, D.J., Swaroop, A., 2000. The Leucine zipper of NRL interacts with the CRX Homeodomain: a possible mechanism of transcriptional synergy in rhodopsin regulation. *J. Biol. Chem.* 275, 29794–29799. <https://doi.org/10.1074/jbc.M003658200>.
- Nathans, J., Thomas, D., Hogness, D.S., 1986. Molecular genetics of human color vision: the genes encoding blue, green, and red pigments. *Science* 232, 193–202.
- National Eye Institute Commons, (NEI) 2017. <https://neicommons.nei.nih.gov> (accessed 9.14.20).
- Nishida, A., Furukawa, A., Koike, C., Tano, Y., Aizawa, S., Matsuo, I., Furukawa, T., 2003. *Otx2* homeobox gene controls retinal photoreceptor cell fate and pineal gland development. *Nat. Neurosci.* 6, 1255–1263. <https://doi.org/10.1038/nn1155>.
- Oh, E.C.T., Khan, N., Novelli, E., Khanna, H., Strettoi, E., Swaroop, A., 2007. Transformation of cone precursors to functional rod photoreceptors by bZIP transcription factor NRL. *Proc. Natl. Acad. Sci. U. S. A.* 104, 1679–1684. <https://doi.org/10.1073/pnas.0605934104>.
- Oh, E.C.T., Cheng, H., Hao, H., Jia, L., Khan, N.W., Swaroop, A., 2008. Rod differentiation factor NRL activates expression of nuclear receptor NR2E3 to suppress the development of cone photoreceptors. *Brain Res.* 1236, 16–29. <https://doi.org/10.1016/j.brainres.2008.01.028>.
- Onishi, A., Peng, G.H., Hsu, C., Alexis, U., Chen, S., Blackshaw, S., 2009. Pias3-dependent SUMOylation directs rod photoreceptor development. *Neuron* 61, 234–246. <https://doi.org/10.1016/j.neuron.2008.12.006>.
- Peng, G.H., Ahmad, O., Ahmad, F., Liu, J., Chen, S., 2005. The photoreceptor-specific nuclear receptor Nr2e3 interacts with Crx and exerts opposing effects on the transcription of rod versus cone genes. *Hum. Mol. Genet.* 14, 747–764. <https://doi.org/10.1093/hmg/ddi070>.
- Qin, Q., Knapinska, A., Dobri, N., Madoux, F., Chase, P., Hodder, P., Petrukhin, K., 2013. In pursuit of synthetic modulators for the orphan retina-specific nuclear receptor NR2E3. *J. Ocul. Pharmacol. Ther.* 29, 298–309. <https://doi.org/10.1089/jop.2012.0135>.
- Raj, B., Blencowe, B.J., 2015. Alternative splicing in the mammalian nervous system: recent insights into mechanisms and functional roles. *Neuron* 87, 14–27. <https://doi.org/10.1016/j.neuron.2015.05.004>.
- Ray, T.A., Cochran, K., Kozlowski, C., Wang, J., Alexander, G., Cady, M.A., Spencer, W.J., Ruzycski, P.A., Clark, B.S., Laeremans, A., He, M.X., Wang, X., Park, E., Hao, Y., Iannaccone, A., Hu, G., Fedrigo, O., Skiba, N.P., Arshavsky, V.Y., Kay, J.N., 2020. Comprehensive identification of mRNA isoforms reveals the diversity of neural cell-surface molecules with roles in retinal development and disease. *Nat. Commun.* 11, 3328. <https://doi.org/10.1038/s41467-020-17009-7>.
- RetNet, 1996-2020 <https://sph.uth.edu/retnet/> (accessed 2.21.20).
- Reyes, A., Huber, W., 2018. Alternative start and termination sites of transcription drive most transcript isoform differences across human tissues. *Nucleic Acids Res.* 46, 582–592. <https://doi.org/10.1093/nar/gkx1165>.
- Reyes-Resina, I., Alkozi, H.A., Del Ser-Badía, A., Sánchez-Naves, J., Lillo, J., Jiménez, J., Pintor, J., Navarro, G., Franco, R., 2020. Expression of melatonin and dopamine D3 receptor heteromers in eye ciliary body epithelial cells and negative correlation with ocular hypertension. *Cells* 9, 152. <https://doi.org/10.3390/cells9010152>.
- Roduit, R., Escher, P., Schorderet, D.F., 2009. Mutations in the DNA-binding domain of NR2E3 affect in vivo dimerization and interaction with CRX. *PLoS One* 4, 1–12. <https://doi.org/10.1371/journal.pone.0007379>.
- Roesch, K., Stadler, M.B., Cepko, C.L., 2012. Gene expression changes within Müller glial cells in retinitis pigmentosa. *Mol. Vis.* 18, 1197–1214.
- Schnapf, J.L., Kraft, T.W., Baylor, D.A., 1987. Spectral sensitivity of human cone photoreceptors. *Nature* 325, 439–441.
- Schorderet, D.F., Escher, P., 2009. NR2E3 mutations in enhanced S-cone sensitivity syndrome (ESCS), Goldmann-Favre syndrome (GFS), clumped pigmentary retinal degeneration (CPRD), and retinitis pigmentosa (RP). *Hum. Mutat.* 30, 1475–1485. <https://doi.org/10.1002/humu.21096>.
- Smith, P.J., Zhang, C., Wang, J., Chew, S.L., Zhang, M.Q., Krainer, A.R., 2006. An increased specificity score matrix for the prediction of SF2/ASF-specific exonic splicing enhancers. *Hum. Mol. Genet.* 15, 2490–2508. <https://doi.org/10.1093/hmg/ddl171>.
- Suzuki, S.C., Bleckert, A., Williams, P.R., Takechi, M., Kawamura, S., Wong, R.O.L., 2013. Cone photoreceptor types in zebrafish are generated by symmetric terminal divisions of dedicated precursors. *Proc. Natl. Acad. Sci. U. S. A.* 110, 15109–15114. <https://doi.org/10.1073/pnas.1303551110>.
- Swaroop, A., Kim, D., Forrest, D., 2010. Transcriptional regulation of photoreceptor development and homeostasis in the mammalian retina. *Nat. Rev. Neurosci.* 11, 563–576. <https://doi.org/10.1038/nrn2880>.
- SWISS-Model EXPASY, 2017. <https://swissmodel.expasy.org> (accessed 5.3.20).
- Taliaferro, J.M., Vidaki, M., Oliveira, R., Olson, S., Zhan, L., Saxena, T., Wang, E.T., Graveley, B.R., Gertler, F.B., Swanson, M.S., Burge, C.B., 2016. Distal alternative last exons localize mRNAs to neural projections. *Mol. Cell* 61, 821–833. <https://doi.org/10.1016/j.molcel.2016.01.020>.
- Tan, M.H.E., Zhou, X.E., Soon, F.F., Li, X., Li, J., Yong, E.L., Melcher, K., Xu, H.E., 2013. The crystal structure of the orphan nuclear receptor NR2E3/PNR ligand binding domain reveals a dimeric auto-repressed conformation. *PLoS One* 8, 1–13. <https://doi.org/10.1371/journal.pone.0074359>.
- Toulis, V., Garanto, A., Marfany, G., 2016. Combining zebrafish and mouse models to test the function of deubiquitinating enzyme (DUB) genes in development: role of *USP45* in the retina. In: Matthies, R. (Ed.), *Proteostasis: Methods and Protocols*. Springer New York, New York, NY, pp. 85–101. [https://doi.org/10.1007/978-1-4939-3756-1\\_3](https://doi.org/10.1007/978-1-4939-3756-1_3).
- Turner, D.L., Snyder, E.Y., Cepko, C.L., 1990. Lineage-independent determination of cell type in the embryonic mouse retina. *Neuron* 4, 833–845. [https://doi.org/10.1016/0896-6273\(90\)90136-4](https://doi.org/10.1016/0896-6273(90)90136-4).
- Ueno, S., Kondo, M., Miyata, K., Hirai, T., Miyata, T., Usukura, J., Nishizawa, Y., Miyake, Y., 2005. Physiological function of S-cone system is not enhanced in *rd7* mice. *Exp. Eye Res.* 81, 751–758. <https://doi.org/10.1016/j.exer.2005.04.013>.
- von Alpen, D., Tran, H.V., Guex, N., Venturini, G., Munier, F.L., Schorderet, D.F., Haider, N.B., Escher, P., 2015. Differential dimerization of variants linked to enhanced S-cone sensitivity syndrome (ESCS) located in the NR2E3 ligand-binding domain. *Hum. Mutat.* 36, 599–610. <https://doi.org/10.1002/humu.22775>.
- Walls, G.L., 1943. The vertebrate eye and its adaptive radiation. *Nature* 151, 236. <https://doi.org/10.5962/bhl.title.7369>.
- Webber, A.L., Hodor, P., Thut, C.J., Vogt, T.F., Zhang, T., Holder, D.J., Petrukhin, K., 2008. Dual role of *Nr2e3* in photoreceptor development and maintenance. *Exp. Eye Res.* 87, 35–48. <https://doi.org/10.1016/j.exer.2008.04.006>.
- Wright, A.F., Reddick, A.C., Schwartz, S.B., Ferguson, J.S., Aleman, T.S., Kellner, U., Jurklics, B., Schuster, A., Zrenner, E., Wissinger, B., Lennon, A., Shu, X., Cideciyan, A.V., Stone, E.M., Jacobson, S.G., Swaroop, A., 2004. Mutation analysis of *NR2E3* and *NRL* genes in enhanced S cone syndrome. *Hum. Mutat.* 24, 439. <https://doi.org/10.1002/humu.9285>.
- Xie, S., Han, S., Qu, Z., Liu, F., Li, J., Yu, S., Reilly, J., Tu, J., Liu, X., Lu, Z., Hu, X., Yimer, T.A., Qin, Y., Huang, Y., Lv, Y., Jiang, T., Shu, X., Tang, Z., Jia, H., Wong, F., Liu, M., 2019. Knockout of *Nr2e3* prevents rod photoreceptor differentiation and leads to selective L-/-M-cone photoreceptor degeneration in zebrafish. *Biochim. Biophys. Acta Mol. Basis Dis.* 1865, 1273–1283. <https://doi.org/10.1016/j.bbadis.2019.01.022>.
- Yoshida, S., Mears, A.J., Friedman, J.S., Carter, T., He, S., Oh, E., Jing, Y., Farjo, R., Fleury, G., Barlow, C., Hero, A.O., Swaroop, A., 2004. Expression profiling of the developing and mature *Nrl* -/- mouse retina: identification of retinal disease candidates and transcriptional regulatory targets of *Nrl*. *Hum. Mol. Genet.* 13, 1487–1503. <https://doi.org/10.1093/hmg/ddh160>.